



PONTIFICIA
**UNIVERSIDAD
CATÓLICA**
DEL PERÚ

tu
TECHNISCHE UNIVERSITÄT
ILMENAU

Pontificia Universidad Católica del Perú

Escuela de Posgrado

Master Thesis

Implementation of a four probes measuring system to
determine the resistivity of thin films with temperature
dependence

Para optar el grado de:

Magister en:

Ingeniería Mecatrónica

Presentado por: Carlos Alberto Salas Casapino

Asesor (PUCP): M.Sc. Jorge Andrés Guerra Torres

Asesor (TU Ilmenau): PD Dr.-Ing. habil. Tom Ströhla

Tutor: Dr.-Ing. Rolf Grieseler

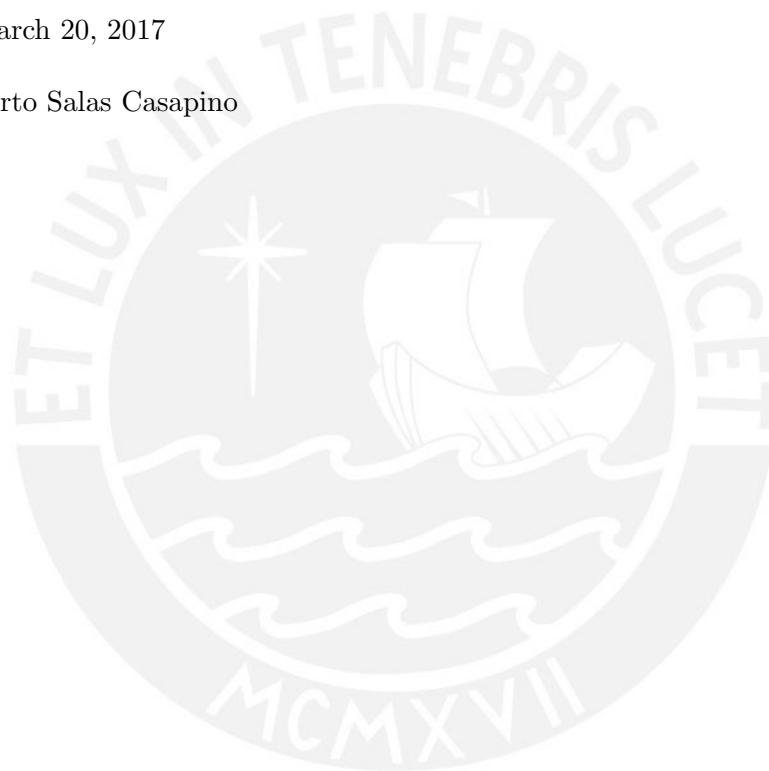
Fecha: 20/03/2017

Statement of Authorship

The present work has been made independently without use other than those specified sources. All points were taken literally or in accordance with their published sources are identified as such. The work has not been submitted in the same or similar form, under one or other tests.

Ilmenau, March 20, 2017

Carlos Alberto Salas Casapino



Abstract

Resistivity measurements in thin film samples depending on the temperature and on the film thickness is always a subject of interest, above all when it comes to new materials.

This work presents the implementation of a measuring system for thin film resistivity based on four probes showing the dependency of the resistivity on the temperature as well as on the film thickness. In order to change the temperature of the samples, a heat source based on a Peltier element was implemented into the measuring system. A Graphical User Interface using a LabVIEW software controls all the devices of the measuring system and allows the user to calculate the thin film resistivity choosing between four measuring method: Van der Pauw, Modified Van der Pauw, Linear Van der Pauw and Linear Four Probes methods.

Resistivity in aluminum and tungsten thin film samples with 100, 300, and 600 nm thickness were measured at temperatures between 303 K and 373 K with increments of 5 K. The results obtained are higher than bulk resistivity values and agrees with the present theory. Moreover, it is shown that the resistivity values obtained and its corresponding temperature coefficients increases as the film thickness decreases.

Resumen

La medición de la resistividad en láminas delgadas dependiendo de la temperatura así como del espesor de lámina es siempre un tema de interés, sobretodo cuando se trata de nuevos materiales.

Este trabajo presenta la implementación de un sistema de medición de resistividad en láminas delgadas basado en cuatro puntas que muestra la dependencia de la resistividad con respecto a la temperatura, así como al espesor de lámina. Con el fin de cambiar la temperatura en la muestra, una fuente de calor basada en un elemento Peltier fue implementada dentro del sistema de medición. Una Interfaz Gráfica de Usuario desarrollada en LabVIEW controla todos los equipos del sistema de medición y permite al usuario calcular la resistividad en láminas delgadas escogiendo entre cuatro métodos de medición: el método de Van der Pauw, el método de Van der Pauw modificado, el método de Van der Pauw linear y el método de las Cuatro Puntas Lineales.

Se realizaron mediciones de resistividad en láminas delgadas de aluminio y tungsteno con espesores de 100, 300 y 600 nm, respectivamente, dentro de un rango de temperaturas de 303 K Y 373 K con incrementos de 5 K. Los resultados obtenidos indican que los valores de resistividad en láminas delgadas son mayores que los valores de resistividad en muestras a granel (bulk) concordando con la teoría. Así mismo, se muestra que los valores de resistividad medidos y sus respectivos coeficientes de temperatura se incrementan a medida que el espesor de lámina delgada decrece.

Zusammenfassung

Die Messungen des Schichtwiderstandes von dünnen Schichten in Abhängigkeit von der Temperatur und der Dicke der Schichten ist ein interessantes Thema, vor allem, wenn es um neuen Materialien geht.

Die vorliegende Arbeit befasst sich mit der Umsetzung eines Messungssystems für die Messung des Schichtwiderstandes von dünnen Schichten. Dieses basiert auf unterschiedlichen Methoden der Vierspitzenmessung. Mit dem Ziel die Temperatur der zu untersuchenden Proben zu ändern, wurde eine Wärmequelle basierend auf einem Peltier-Element ins Messsystem implementiert. Unter Verwendung einer LabVIEW-Software kontrolliert der Nutzer mittels einer graphischen Benutzeroberfläche alle Messgeräte. Weiterhin wird durch die Software der elektrische Widerstand der dünnen Schichten berechnet. Zur Bestimmung des Schichtwiderstandes kann eine der vier implementierten Messmethoden genutzt werden: die Van der Pauw Methode, die modifizierte Van der Pauw Methode, die Linear Van der Pauw Methode und die Linear Vierspitzenmessung Methode.

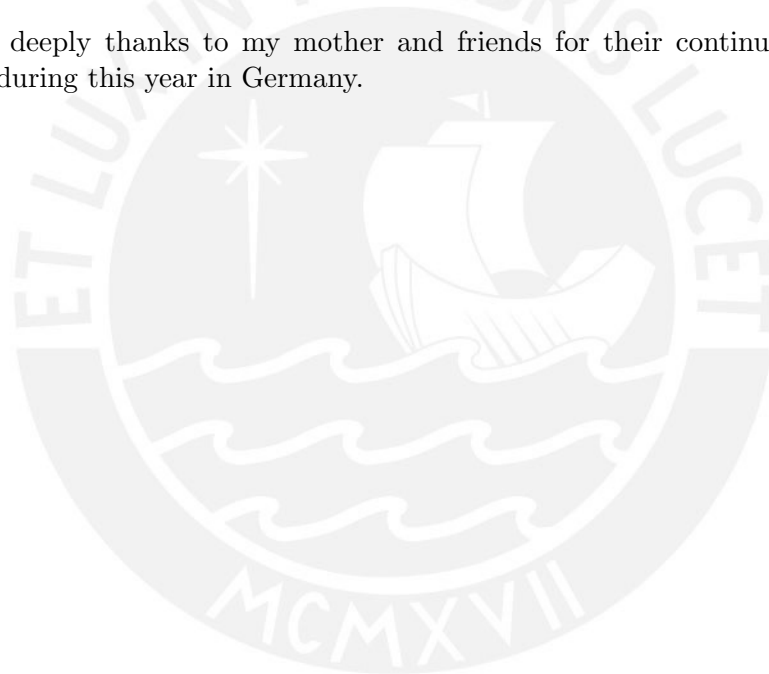
Der elektrische Widerstand wurde an verschiedenen Proben mit Aluminium- und Wolframschichten und einer Schichtdicke von 100, 300 und 600 nm gemessen. Die Temperaturen wurden dabei zwischen 303 K und 373 K in Schritten von 5 K gemessen. Die Ergebnisse liegen über den Werten für den spezifische Widerstand der Vollmaterialien stimmen aber mit der gezeigten Theorie überein. Weiterhin konnte gezeigt werden, dass die erhaltenen Widerstandswerte und die entsprechenden Temperaturkoeffizienten steigen, je geringer die Schichtdicke ist.

Acknowledgements

I would like to thank all the people who I have met and worked with while writing this thesis. My special thanks to my advisors Dr.-Ing. Rolf Grieseler, M.Sc. Andrés Guerra, and PD Dr.-Ing. habil. Tom Ströhla for their continuous guide and valuable support during this work.

I would also like to thank CONCYTEC for the financial support and the opportunity to do a double master's degree at PUCP and at TU Ilmenau.

Finally, my deeply thanks to my mother and friends for their continuous support and motivation during this year in Germany.



Contents

1	Introduction	1
1.1	Motivation	1
1.2	Task assignments	1
1.3	Overview	2
2	State of the art	3
2.1	Dependence of electrical resistivity on temperature	3
	Temperature dependence of electrical resistivity in metals	4
	Temperature dependence of electrical resistivity in semiconductors	5
2.2	Thickness dependence of electrical resistivity and temperature coefficient	6
2.3	Four probes methods for electrical resistivity measurement	8
	Van der Pauw method	8
	Modified Van der Pauw method	10
	Linear Van der Pauw method	12
	Linear Four probes method	12
	Comparison between the methods	17
2.4	Sputtering technique	19
2.5	Thermoelectric Elements	19
	Seebeck Effect	20
	Peltier Effect	21
	Thomson Effect	21
2.6	Control for temperature process	21
	On-off controller	21
	PID controller	22
	Ziegler-Nichols method based on reaction curve	23
2.7	Commercial designs of systems for resistivity measuring	24
3	Design and implementation of the measurement system	25
3.1	Description of the Hardware	25
3.2	Preparation and description of the samples	30
3.3	Temperature control	30
3.4	Description of the Software	34
4	Experimental results	59
4.1	Characterization of the Peltier element	59
4.2	Temperature distribution at the surface of the Peltier element	61
4.3	Temperature distribution in the sample	63
4.4	Resistivity measurements results	67
5	Conclusions	74

Chapter 1

Introduction

1.1 Motivation

The electrical, as well as the thermal behavior of electrical conductive and semiconductive thin films, is always of a wider interest especially when it comes to new materials. Therefore, appropriate measuring techniques are required that give insight into the electrical behavior regarding elevated temperatures.

The electrical resistivity is one of the most important electrical properties in thin film materials. Crucial information like charge carrier concentration and carrier mobility of thin film materials can be retrieved in a rather straight forward procedure through resistivity measurements. Currently, exist several resistivity measurement techniques, among them, Van der Pauw and Four Probes are the most accurate and widely used [1]. Furthermore, some researchers have implemented different modifications of these methods as S. Lim *et al.* [2], who presented a Modified Van der Pauw method for measuring resistivity placing the probes distant from the sample's boundary and S. Thorsteinsson *et al.* [3], who presented an alternative Van der Pauw method placing the four probes along a symmetry line of the sample. Nevertheless, the selection of an appropriate resistivity measurement method will depend on the shape and morphology of the sample.

This thesis focuses on the implementation of a 4 probe measuring system to determine the sheet resistance of thin film samples showing the dependency of the resistivity on the film thickness as well as on the measuring temperature. A Graphical User Interface (GUI) was designed for the measuring system using a LabVIEW software allowing the user to choose between four resistivity measurement methods: Van der Pauw, Modified Van de Pauw, Linear Van der Pauw and Linear Four Probes, and calculate the sheet resistance and resistivity depending on the temperature and thin film thickness using different heating ratios.

1.2 Task assignments

The aim of this thesis is the implementation of a four probes measuring system to determine the resistivity of thin films samples showing the dependency of the resistivity on the film thickness as well as on the measuring temperature. To fulfill this task, the following topics will be examined in the present work:

- Review the temperature dependence of electrical resistivity theory in conductive and semiconductive thin films.

- Review of the state of the art on research concerning thin film resistivity measurement techniques.
- Implement a four probes measuring system as well as a heat source based on a Peltier element using a LabVIEW based program.
- Evaluate the measuring system on thin film samples with different thickness and validate the results with literature.

1.3 Overview

The content of the present thesis is organized as follows:

- *Chapter 2* presents a brief explanation of temperature dependence on thin film measurements, as well as, a summarize of the most used four probes resistivity measuring methods. Furthermore, related concepts to this work like thermoelectric elements, temperature controllers and sputtering technique to obtain thin film samples are also presented in this Chapter.
- *Chapter 3* deals with the design and implementation of the measurement system. The hardware, preparation of the thin film sample, temperature control in the heat source and therefore in the sample, and the software are described in detail in this section.
- *Chapter 4* presents the electrical characterization of the Peltier element, as well as, the temperature distribution at the hot side of the Peltier element and at the surface of the thin film sample. Moreover, resistivity measurements in aluminum and tungsten thin film samples obtained by using the four different methods depending on the temperature and film thickness are shown in this section.
- *Chapter 5* presents the conclusions and the possible future topics of research.

Chapter 2

State of the art

2.1 Dependence of electrical resistivity on temperature

Electrical resistivity is an inherent property of materials that quantifies how well a material retards the flow of electric current [4]. Depending on their values, materials are classified as conductors (metals), semiconductors or insulators [5]. Materials with low resistivity, typically $< 10^{-4} \Omega \text{ cm}$, are considered as conductors and are characterized by the increase in their resistivity values as the temperature rises. Materials with an intermediate range of resistivity, from 10^{-3} to $10^{11} \Omega \text{ cm}$, are considered as semiconductors. Finally, materials with high resistivity, typically $> 10^{12} \Omega \text{ cm}$, that are almost independent of temperature are classified as insulators [6]. Some resistivity values of typical specimens of conductors and semiconductors taking into account the change of temperature are shown in Figure 2.1.

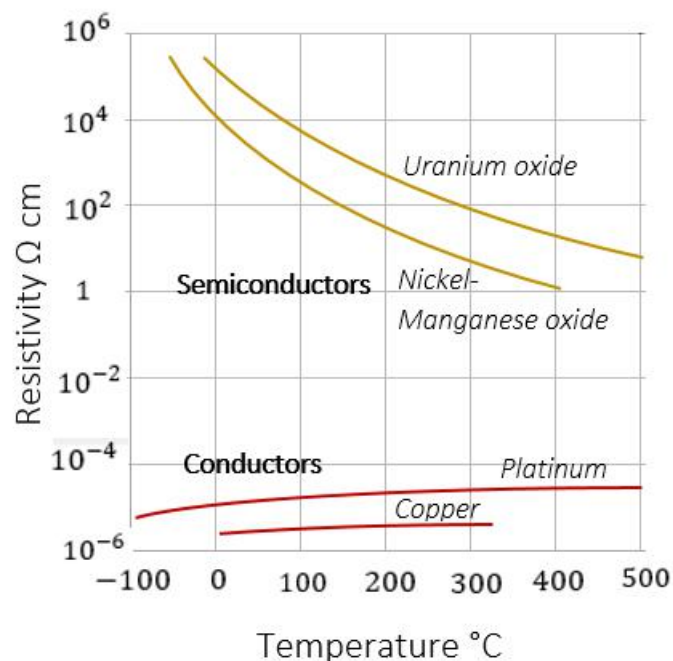


Figure 2.1: Electrical resistivity values of conductors and semiconductors change with temperature variation [7].

Temperature dependence of electrical resistivity in metals

One of the most important characteristics of a metal is the ability to conduct electricity due to the presence of large numbers of quasi-free electrons which under the action of an applied electric field are able to flow through the metallic lattice [8]. The increase of temperature in metals causes the atoms to acquire additional thermal energy and vibrate around their equilibrium position, so that there is more probability of collision between the free electrons and these atoms increasing the electrical resistivity of the conductor [6, 7].

A. Matthiessen *et al.* experimentally found that the total electrical resistivity of a metal depends on two additive contributions: the residual resistivity, ρ_r , caused by the scattering of electrons by impurity atoms and lattice defects; and the intrinsic resistivity, ρ_i , caused by the scattering of electrons by lattice waves or phonons [9, 10], as shown in Equation 2.1. Where $\Delta(c, T)$ is the deviation of the Mattiessen's rule. Figure 2.2 shows the contribution of both: the residual resistivity and the intrinsic resistivity in a metal.

$$\rho(c, T) = \rho_r(c) + \rho_i(T) + \Delta(c, T) \quad (2.1)$$

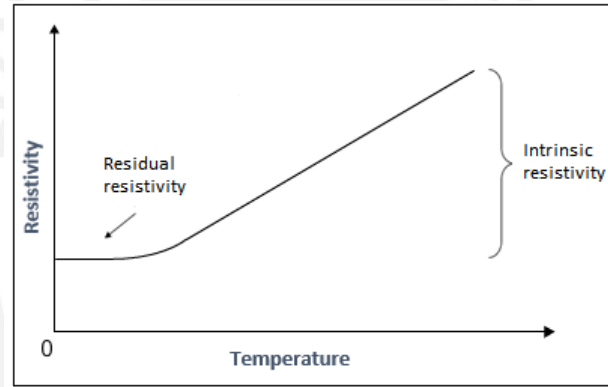


Figure 2.2: Contribution of the residual resistivity and the intrinsic resistivity in a metal. [9].

The residual resistivity, ρ_r , is not temperature dependent but depends on the impurity concentration. The intrinsic resistivity of metals, ρ_i , depends on the temperature and increases approximately linearly when temperature increases [11], as shown in Equation 2.2

$$\rho_i(T) = \rho_o * [1 + \alpha(T - T_o)] \quad (2.2)$$

Where ρ_o is the electrical resistivity of materials at temperature T_o and α is the temperature coefficient of the material.

At elevated temperatures, the behavior of the electrical resistivity in metal shows a progressive increase above the expected values. This effect is attributed to the scattering by thermally generated point defects which add additional atomic sites at high temperatures [12]. In the literature, Equation 2.3 is used to describe approximately the electrical resistivity in metals at high temperatures [13, 14]. Where α and β are the constants characteristic of the metal.

$$\rho_i(T) = \rho_o * [1 + \alpha(T - T_o) + \beta(T - T_o)^2] \quad (2.3)$$

Temperature dependence of electrical resistivity in semiconductors

The electronic structure in a semiconductor is comprised of a conduction band and a valence band. The energy separating the conduction band edge, E_c , and the valence band edge, E_v , is the intrinsic energy gap $E_g = E_c - E_v$ and corresponds to an intrinsic semiconductor [6], as shown in Figure 2.3A. When impurities are added to an intrinsic semiconductor, the electronic band gets new energy levels (E_a, E_d) that modify the Fermi level thus changing the electric properties of the material [11]. The impurity can be an atom having one valence electron more than the semiconductor atom (*donor*) adding an extra energy, E_d , just below the conduction band or an atom with one valence electron less than the semiconductor atom (*acceptor*), adding an extra energy, E_a , just above the valence band [6]; as shown in Figure 2.3 B.

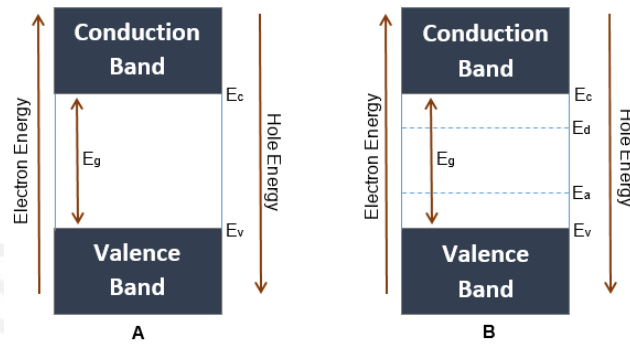


Figure 2.3: Semiconductor electronic bands. **A** represents the energy gap E_g of an intrinsic semiconductor. **B** represents the energy gap E_g of an extrinsic (doped) semiconductor having a donor level E_d and a receptor level E_a [6].

According to C. Michel *et al.* resistivity in extrinsic semiconductors can be approximately described by Arrhenius temperature dependence formula [15], as shown in Equation 2.4

$$\rho = A * e^{\frac{\Delta E}{kT}} \quad (2.4)$$

Where A is a pre-exponential factor, ΔE is the activation energy, k is the Boltzmann constant and T is the absolute temperature. Figure 2.4 gives insight into the behavior of electrical resistivity in semiconductors depending on the temperature [11].

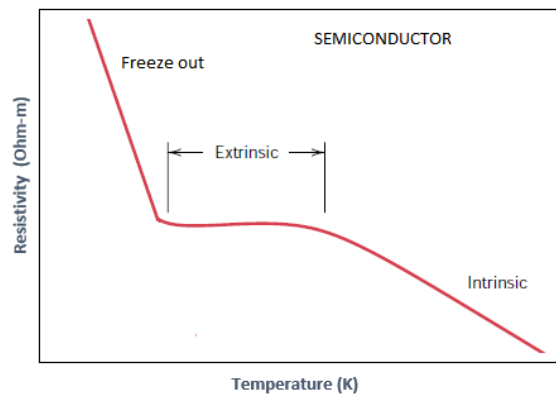


Figure 2.4: Schematic plot of electrical resistivity in semiconductors depending on the temperature.

2.2 Thickness dependence of electrical resistivity and temperature coefficient

In 1938, Fuchs and Sondheimer proposed a model for the influence of the thickness in electrical resistivity of thin film samples. This model is based on the Boltzmann transport equation and associates the behavior of free electrons with a mean free path in the bulk material λ_0 [16,17]. The general expression of this model is shown in Equation 2.5

$$\frac{\rho_0}{\rho_\infty} = 1 - \frac{3}{2\kappa_0} \int_1^\infty \left(\frac{1}{t^3} - \frac{1}{t^5} \right) \frac{1 - e^{-\kappa_0 t}}{1 - p e^{-\kappa_0 t}} dt \quad (2.5)$$

Where ρ_∞ is the resistivity of the film to be calculated, ρ_0 is the resistivity of the bulk material, $\kappa_0 = d/\lambda_0$ is the ratio between the mean film thickness and the mean free path in the bulk material, and p is a the specularity parameter. The specularity parameter, p , will depend on the film preparation method (sputtering, epitaxial growth) and the substrate where the film has been deposited. This general equation can be simplified in Equation 2.6 for sufficiently high κ_0 values $d \ll \lambda_0$ [11].

$$\frac{\rho_0}{\rho_\infty} = 1 + \frac{3}{8\kappa_0} (1 - p) \quad (2.6)$$

A more simplified calculation of the resistivity of a conducting thin film modifies the specularity parameter, p , and the constants from Equation 2.6 by a numerical factor $1/\pi$, as shown in Equation 2.7 [11].

$$\frac{\rho_0}{\rho_\infty} = 1 + \frac{1}{\pi\kappa_0} \quad (2.7)$$

Figure 2.5 shows the resistivity curve of Cu polycrystalline samples versus film thickness. The results are compared with its corresponding bulk resistivity.

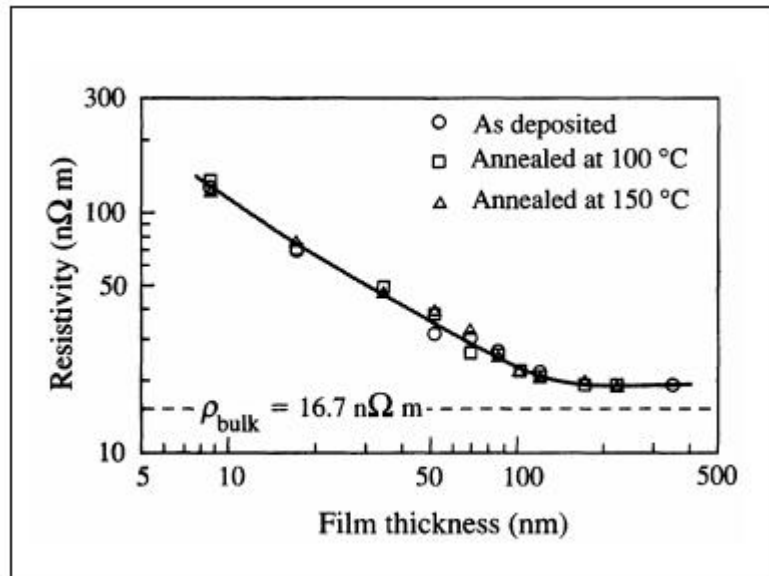


Figure 2.5: Resistivity vs. thickness plot of Cu polycrystalline thin films [11].

The behavior of the temperature coefficient of thin metal films depending on the thickness was derived from the Fuch-Sondheimer size effect theory for $d > 0.1\lambda$ [18,19], as shown in Equation 2.8.

$$\alpha_{\infty} = \alpha_0 \left(1 - \frac{3\lambda}{8d}(1-p)\right) \quad (2.8)$$

Where λ is the intrinsic mean free path and d is the thickness of the sample. Figure 2.6 shows the temperature coefficient curve for different metals showing their thickness dependency.

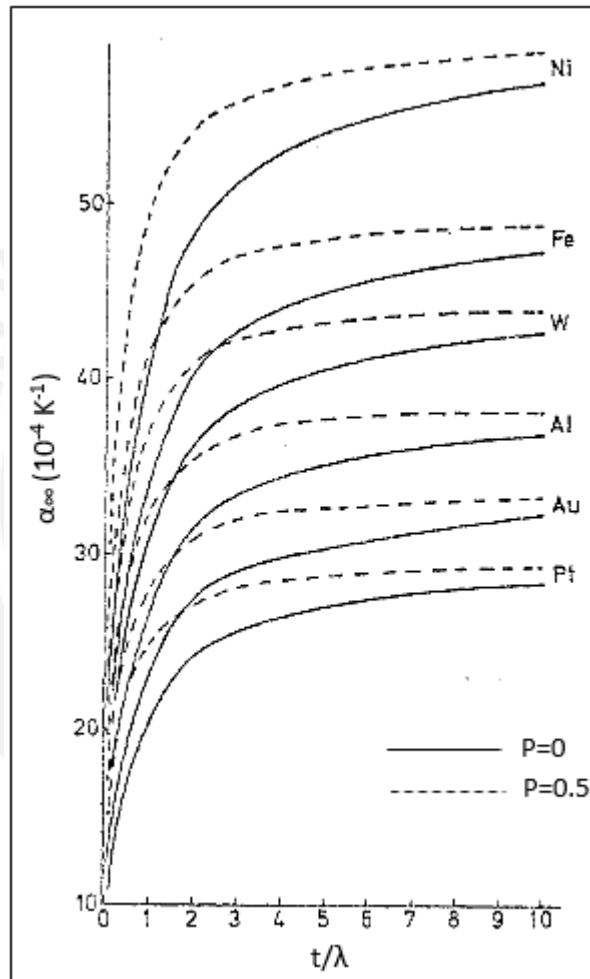


Figure 2.6: Temperature coefficient vs. thickness plot of different conductors [20].

2.3 Four probes methods for electrical resistivity measurement

Various methods have been suggested to measure the electrical resistivity, among them methods using two and four probes. Four probes methods are probably the most outstanding due to the fact that they do not take into account the effects of contact resistance between the sample and the electrical contacts that allow obtaining more accurate and reliable results [21]. A summary of four methods based on four probes: Van der Pauw, Linear Van der Pauw, Modified Van der Pauw and Linear Four Point Probes, is presented below.

Van der Pauw method

Van der Pauw method is one of the most effective and widely used technique for measuring the resistivity of thin films with substrates having an arbitrary shape [1]. This method is applicable when the following conditions are satisfying [22]:

- The contacts are at the circumference of the sample.
- The contacts are sufficiently small.
- The sample is homogeneous in thickness.
- The surface of the sample is singly connected. That is, the sample does not have isolated holes.

Considering a flat sample with an arbitrary shape where successive contacts A, B, C, and D are placed along the circumference, as shown in Figure 2.7, Van der Pauw established a general relationship, shown in Equation 2.9, to obtain the resistivity of the sample.

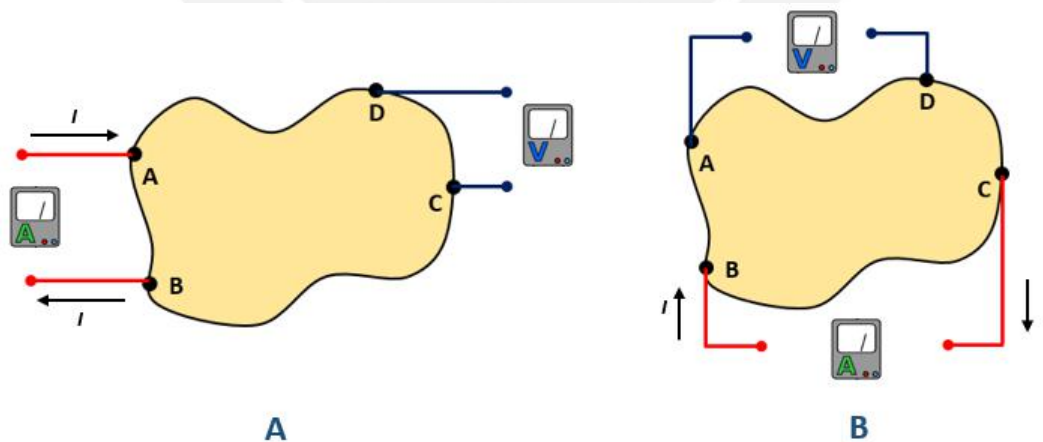


Figure 2.7: Electrical configuration for Van der Pauw method. **A** represents the configuration to obtain the resistance $R_{AB,CD}$, while **B** represents the configuration to obtain the resistance $R_{BC,DA}$ [22].

$$e^{-\frac{\pi d}{\rho} R_{AB,CD}} + e^{-\frac{\pi d}{\rho} R_{BC,DA}} = 1 \quad (2.9)$$

The resistance $R_{AB,CD}$ is defined as the potential difference $V_D - V_C$ between the contacts D and C per unit of current through the contacts A and B . The current enters the sample through the contact A and leaves it through the contact B . Analog, resistance $R_{BC,DA}$ is obtained switching the contacts, as show in Figure 2.7 B , where $V_A - V_D$ is the potential difference between the contacts A and D per unit of current through the contacts B and C . Finally, ρ is the resistivity value and d is the thickness of the sample.

In order to simplify the solution of the resistivity ρ , Van der Pauw rewrites Equation 2.9 as a function of $R_{AB,CD}$ and $R_{BC,DA}$ and the thickness d .

$$\rho = \frac{\pi d}{\ln 2} \left(\frac{R_{AB,CD} + R_{BC,DA}}{2} \right) f\left(\frac{R_{AB,CD}}{R_{BC,DA}}\right) \quad (2.10)$$

Where $f\left(\frac{R_{AB,CD}}{R_{BC,DA}}\right)$ is a Van der Pauw's function of the ratio $\frac{R_{AB,CD}}{R_{BC,DA}}$ and satisfies the relation 2.11

$$\frac{R_{AB,CD} - R_{BC,DA}}{R_{AB,CD} + R_{BC,DA}} = \frac{f}{\ln 2} \operatorname{arccosh}\left(\frac{e^{\frac{\ln 2}{f}}}{2}\right) \quad (2.11)$$

Equation 2.9 can be simplified for samples that present a plane of symmetry when two probes are placed on the line of the symmetry and the other two are placed symmetrically with respect to this line, as shown in Figure 2.8.

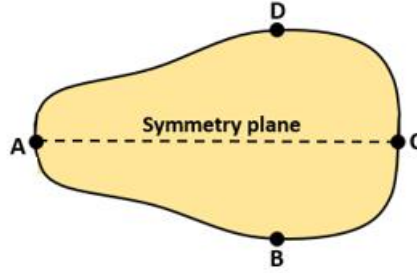


Figure 2.8: Configuration for Van der Pauw method applied in a symmetrical sample [5].

This configuration allows to obtain $R_{AB,CD} = R_{BC,DA} = R$ and the resistivity is expressed as:

$$\rho = \frac{\pi d}{\ln 2} \left(\frac{V}{I} \right) \quad (2.12)$$

Modified Van der Pauw method

One of the conditions for the Van der Pauw method assumes that the contacts must be placed at the boundaries of the sample. In some particular situations, it is difficult to place a contact of very small area exactly on the edge of the sample. In view of this situation, S.Lim *et al.* presented an algorithm which follows the original Van der Pauw derivation but with the assumption that the contacts are placed at a distance away from the boundary [2].

To obtain the new equation, Lim *et al.* assumes an infinite plane with four contacts A' , B' , C' , and D' along a straight line and a current $2i$ injected at contact A' , as shown in Figure 2.9 Part A. The current has a radial distribution around A' and $V_{D'} - V_{C'}$ is calculated. Then, Lim *et al.* assumed that the current $2i$ is extracted from contact B' and $V_{D'} - V_{C'}$ is calculated. Taking into account the principle of superposition, $V_{D'} - V_{C'}$ is calculated for the case where the current $2i$ is injected at A' and extracted at B' , as shown in Figure 2.9 Part B. In order to obtain the resistance $R_{A'B',C'D'}$, $V_{D'} - V_{C'}$ is divided by the current $2i$ obtaining the Equation 2.13. Accordingly, resistance $R_{B'C',D'A'}$ value is obtained, shown in Equation 2.14.

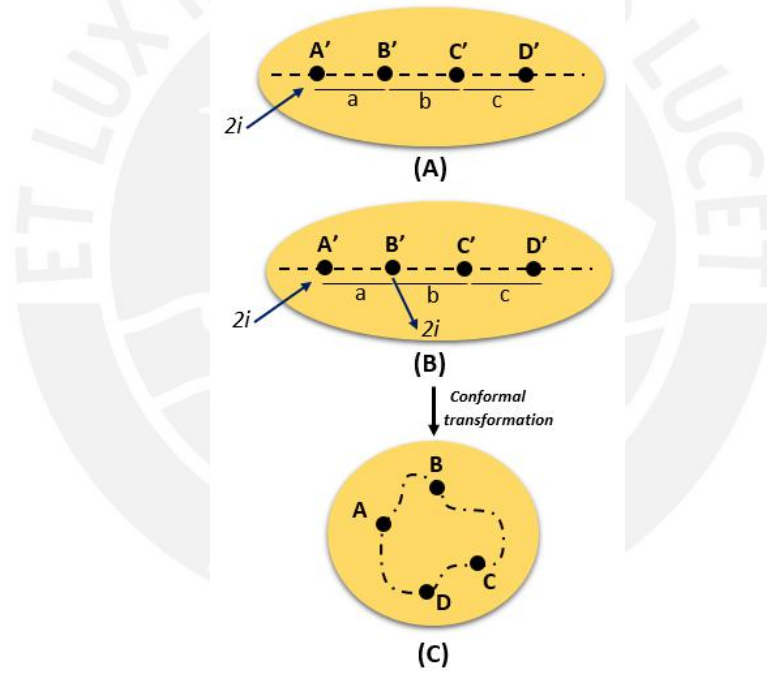


Figure 2.9: **A)** $A'B'C'D'$ are the positions of the contacts in a straight line, where a current $2i$ is injected in contact A' . **B)** A current $2i$ is injected in contact A' and extracted in contact B' . **C)** Conformal transformation mapped contacts A' , B' , C' , and D' which form a straight line directly to arbitrary locations A , B , C , and D [2].

$$\frac{b(a+b+c)}{(a+b)(b+c)} = e^{\frac{-2\pi d}{\rho} R_{A'B',C'D'}} \quad (2.13)$$

$$\frac{ac}{(a+b)(b+c)} = e^{\frac{-2\pi d}{\rho} R_{B'C',D'A'}} \quad (2.14)$$

Combining Equations 2.13 and 2.14, Lim *et al.* obtained an alternative expression of Van der Pauw method for contacts A' , B' , C' , and D' which form a straight line. In order to apply this equation to contacts A , B , C , and D placed in arbitrary locations on a 2D infinite plane, a conformal transformation is proposed by the authors, as shown in Figure 2.9 Part C. The resulting expression for this modified Van der Pauw method is shown in Equation 2.15, where the resistances calculated by this method are equivalent to the resistances calculated by the original Van der Pauw method. The advantage of this new method is that it is easier to achieve and eliminates errors associated to contacts that are not placed exactly at the edge of the sample.

$$e^{-2\frac{\pi d}{\rho}R_{AB,CD}} + e^{-2\frac{\pi d}{\rho}R_{BC,DA}} = 1 \quad (2.15)$$

Lim *et al.* conducted an experiment to assess the error in the resistivity calculation using the modified Van der Pauw formulation 2.15. These results are shown in Figure 2.10 and present the relation between the area and the resistivity of an aluminum sample doped with ZnO, and compare the results obtained with the original Van der Pauw formula (■) and those obtained with the modified formula (●). According to the results obtained by the authors, the measurements with the modified method are more accurate when the contacts are more distant from the boundary.

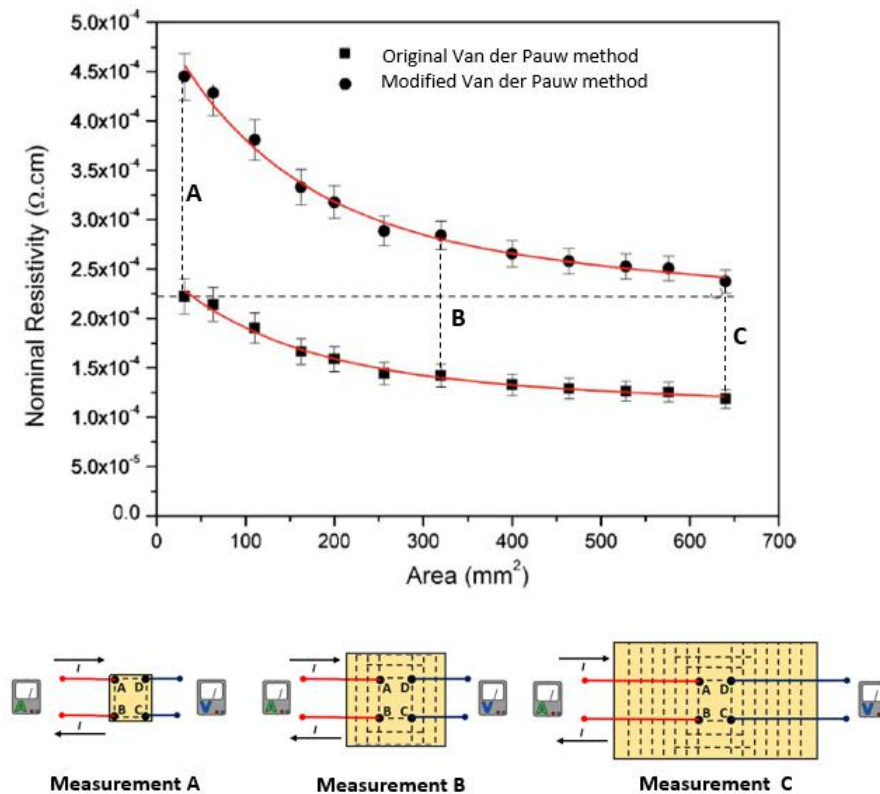


Figure 2.10: Relation between the area and the resistivity of a sample, with theoretical value $2.2 \times 10^{-4} \Omega cm$, obtained with the original Van der Pauw formula (■) and the modified Van der Pauw formula (●). The schematics of the measurements A, B, and C are shown below the graph [2].

Linear Van der Pauw method

Another variation of the Van der Pauw method was elaborated by S. Thorsteinsson *et al.* for samples with one or more planes of symmetry. For this particular samples, the authors experimentally found that the resistance measurements, when the four probes are placed along a symmetry line of the sample, as shown in Figure 2.11, are lowered exactly by a factor of two compared to the situation where the probes are placed on the boundary of the sample [3]. Consequently, the original Van der Pauw equation can be rewritten as Equation 2.16.

$$e^{-2\frac{\pi d}{\rho}} R_{AB,CD} + e^{-2\frac{\pi d}{\rho}} R_{BC,DA} = 1 \quad (2.16)$$

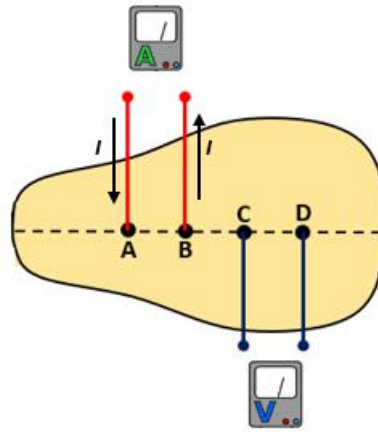


Figure 2.11: Configuration for Linear Van der Pauw method applied in a symmetric sample [5].

In particular measurements, this method results useful when it is difficult to place the probes at the boundary of a symmetrical sample. The spacing between the probes is not taken into account during the tests.

Linear Four probes method

The linear four probes method is considered a classical method for resistivity measurements in infinite 2D thin films [23]. This method consists of placing four probes that make contact along a line on the surface of the sample. Through the two outer pair of probes current is inserted into the sample and voltage is measured across the two inner probes, as shown in Figure 2.12. In order to use this method it is necessary to assume that: the distances between the probes are small compared to the dimension of the sample, none of the probes are too close to the boundary of the sample and the surface on which the probes rest must be flat with no surface leakage [24].

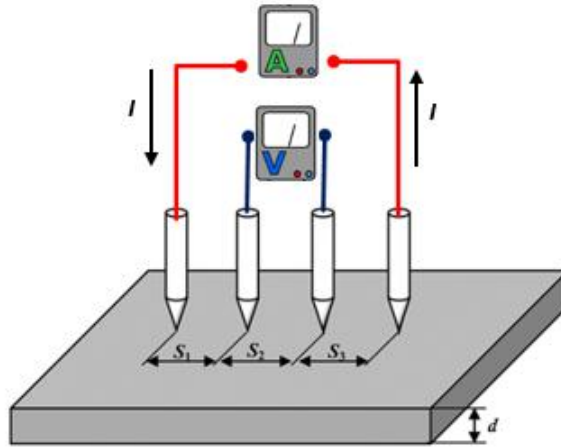


Figure 2.12: Electrical configuration for Linear Four Probes method [25].

According to I. Miccoli *et al.*, for instances when the thickness d of the sample is small compared to the probes spacing, the resistivity of a sample can be expressed in terms of the potential difference and the current [5], as shown in 2.17:

$$\rho = \left(\frac{V}{I}\right) \left(\frac{2\pi}{\ln\left(\frac{(s_2+s_3)(s_1+s_2)}{s_1s_3}\right)}\right) d \quad (2.17)$$

Where V is the voltage measured between the inner probes, I , the current applied to the sample, d , the thickness of the sample and s_1, s_2, s_3 , the distances between the probes. When the probes are equally spaced (with $s_1 = s_2 = s_3 = s$), 2.17 can be represented by:

$$\rho = \left(\frac{V}{I}\right) \left(\frac{\pi}{\ln 2}\right) d \quad (2.18)$$

A variation of this method allows the four probes to be arranged in a squared configuration, as shown in Figure 2.13. This configuration has the advantage of requiring a smaller area for the measurement [5].

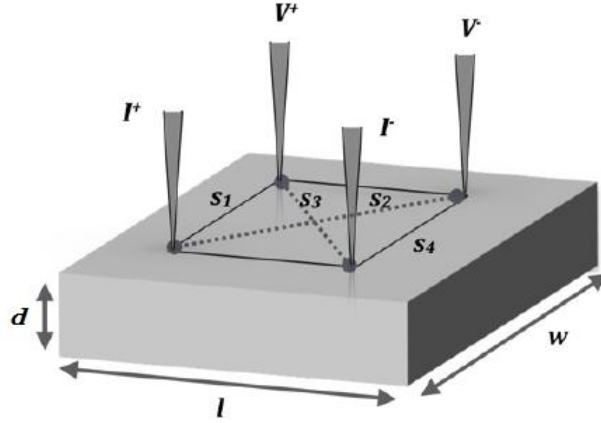


Figure 2.13: Electrical resistivity measurement with the four probes arranged in a square configuration [5].

The corresponding expression for this configuration where $s_1 = s_4 = s$ and $s_2 = s_3 = \sqrt{2}s$ is shown in 2.19:

$$\rho = 2\left(\frac{V}{I}\right)\left(\frac{2\pi}{\ln 2}\right)d \quad (2.19)$$

Where 2.19 differs of 2.18 only by a factor of two.

Correction Factors for Linear Four Probes Method

Electrical resistivity measurements with Linear Four Probes Method require correction factors to correct errors due to the geometry of the sample and the positioning of contacts regarding the boundaries [26]. The resistivity with a correction factor can be expressed as:

$$\rho = F \frac{V}{I} \quad (2.20)$$

Where $F = F_1 * F_2 * F_3$ is the geometric factor. F_1 takes into account the thickness of the sample, F_2 the alignment of the probes in the proximity of a sample edge and F_3 the total lateral width of the sample [5].

Correction Factor 1: Thickness of the sample

The electrical resistivity of a sample of thickness, d , using Linear Four Probe method, can be represented as follows [21]:

$$\rho = \left(\frac{\pi V d}{\ln 2 I}\right) F_1\left(\frac{d}{s}\right) \quad (2.21)$$

Where $F_1\left(\frac{d}{s}\right)$ is the thickness correction factor that depends on the thickness, d , and the probe spacing, s . Equation 2.22 shows a solution for F_1 found by Albers and Berkowitz based on an approximated solution of Laplace equation [27].

$$F_1 = \frac{\ln 2}{\ln \left\{ \frac{\sinh\left(\frac{d}{s}\right)}{\sinh\left(\frac{d}{2s}\right)} \right\}} \quad (2.22)$$

The correction factor $F_1\left(\frac{d}{s}\right)$ curve is shown in Figure 2.14.

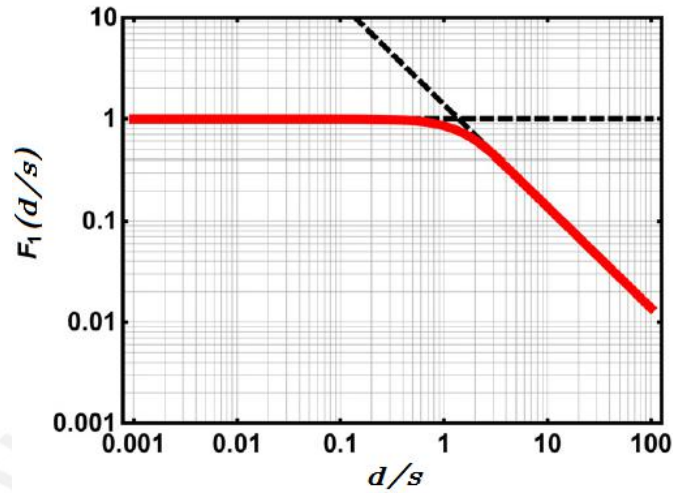


Figure 2.14: Correction factor F_1 where d is the thickness of the sample and s the distance between probes [5].

Correction Factor 2: Probes in the proximity of a single sample edge

During resistivity measuring with Linear Four Probes method, it is necessary to consider a correction factor F_2 produced by errors due to the approach of the probes to the edge of the sample [24]. Figure 2.15 shows a curve for the factor F_2 depending on the ratio between the distance of the probes to the sample edge, a , and the spacing between probes, s .

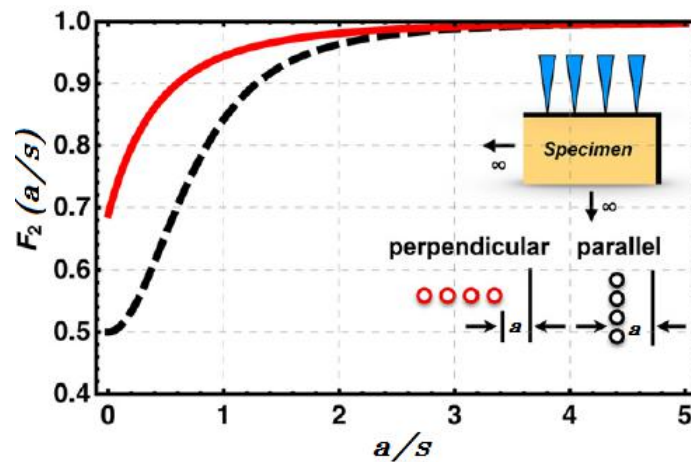


Figure 2.15: Correction factor F_2 where a is the distance of the probes to the sample edge and s the distance between probes [5].

Two possible locations of the probes are taken into account in Figure 2.15: when the probes are perpendicular to the edge and when they are placed parallelly to the edge. The resistivity of a film having the thickness d , measured with the four probes linear method, can be expressed as:

$$\rho = (2\pi s \frac{V}{I}) F_2(\frac{a}{s}) \quad (2.23)$$

Where F_2 , according to L. Valdes, can be expressed as:

$$F_2 = 1 + \frac{s}{2a+s} - \frac{s}{2a+2s} - \frac{1}{2a+4s} + \frac{1}{2a+5s} \quad (2.24)$$

It is important to note that the correction factor F_2 reaches its minimum value $F_{2min} = \frac{1}{2}$ when the four probes array is aligned parallelly along the sample edge [5].

Correction Factor 3: Sample shape

Measurement errors due to the shape of the sample should be taken into account in Four Probe methods [28]. In this section, correction factor F_3 represents sample shape errors and will be described for circular shapes.

When Linear Four Probes method is used and the probe's array is centered with respect to the circular sample, the resistivity can be expressed as:

$$\rho = (\frac{\pi}{\ln 2})(\frac{Vd}{I}) F_3(\frac{D}{s}) \quad (2.25)$$

Where D is the diameter of the sample. Moreover, the correction factor F_3 , according to F. Smits, can be expressed as [28]:

$$F_3 = \frac{\ln 2}{\ln 2 + \ln(\frac{(\frac{D}{s})^2 + 3}{(\frac{D}{s})^2 - 3})} \quad (2.26)$$

A curve for the factor F_3 depending on the sample diameter, D , and the spacing between probes, s , is shown in Figure 2.16.

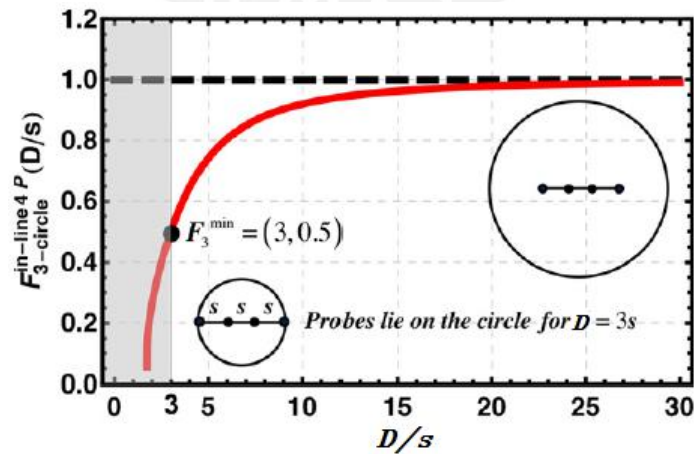


Figure 2.16: Correction factor F_3 where D is the diameter of the sample and s the distance between probes [5].

When the Square Four Probes method is used and the probe's array is placed in the center of the circle, the resistivity can be expressed as:

$$\rho = \left(\frac{2\pi}{\ln 2}\right)\left(\frac{Vd}{I}\right)F_3\left(\frac{D}{s}\right) \quad (2.27)$$

Where D is the diameter of the sample. Furthermore, the correction factor F_3 can be expressed as [5]:

$$F_3 = \frac{\ln 2}{\ln 2 + \ln\left(\frac{(D/s)^2 + 2}{(D/s)^4 - 4}\right)} \quad (2.28)$$

In Figure 2.17 is shown a curve for the factor F_3 depending on the sample diameter D and the square side length s between probes.

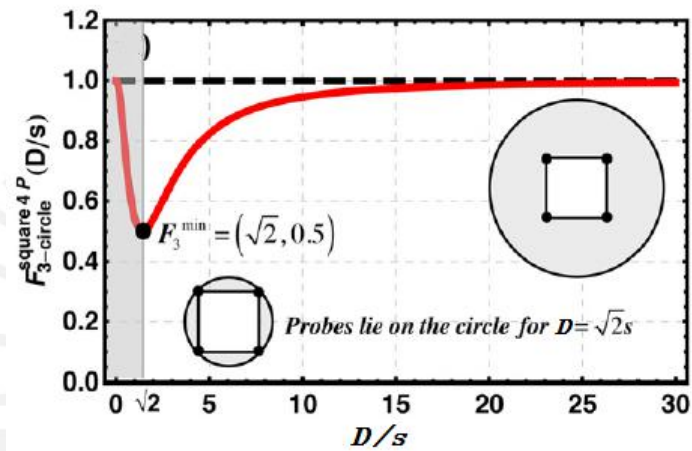
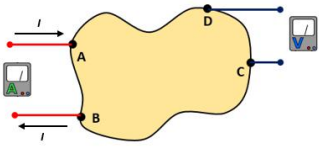
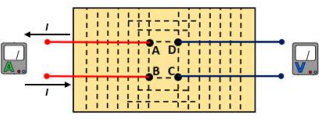
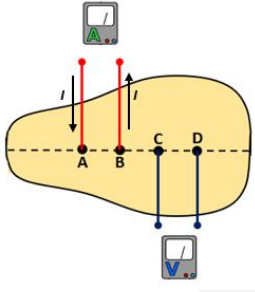
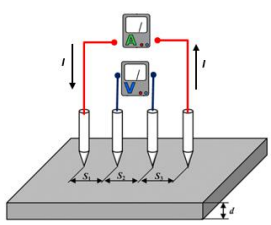
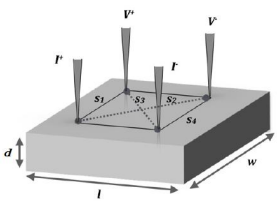


Figure 2.17: Correction factor F_3 where D is the diameter of the sample and s , the side length of the square formed by the probes [5].

Comparison between the methods

Table 2.1 presents the advantages, disadvantages and equations of each method.

Table 2.1: Comparison between methods

Method	Equation	Description
<p>Van der Pauw</p> 	$e^{-\frac{\pi d}{\rho} R_{AB,CD}} + e^{-\frac{\pi d}{\rho} R_{BC,DA}} = 1$	<p>Advantage: Measure samples with arbitrary shapes.</p> <p>Disadvantages: Difficult to place probes at the boundaries.</p>
<p>Modified Van der Pauw</p> 	$e^{-2\frac{\pi d}{\rho} R_{AB,CD}} + e^{-2\frac{\pi d}{\rho} R_{BC,DA}} = 1$	<p>Advantage: Arbitrary shapes. Probes can be placed into the sample.</p> <p>Disadvantages: Experimental results available only for square sample. A correction factor for error is needed. Conformal transformation required.</p>
<p>Linear Van der Pauw</p> 	$e^{-2\frac{\pi d}{\rho} R_{AB,CD}} + e^{-2\frac{\pi d}{\rho} R_{BC,DA}} = 1$	<p>Advantage: Equidistant probes is not mandatory.</p> <p>Disadvantages: Error for probes misalignment. Symmetry shape required.</p>
<p>Linear Four Probes</p> 	$\rho = \left(\frac{V}{I}\right)\left(\frac{\pi}{\ln 2}\right)d$	<p>Advantage: Allows to measure very low resistance values.</p> <p>Disadvantages: Error due to probes misalignment. Correction factor for geometry is required.</p>
<p>Square Four Probes</p> 	$\rho = 2\left(\frac{V}{I}\right)\left(\frac{\pi}{\ln 2}\right)d$	<p>Advantage: Smaller area required than linear method.</p> <p>Disadvantages: Difficult to place probes forming a square. Correction factor for geometry.</p>

2.4 Sputtering technique

The Sputtering technique is a physical vapor deposition (PVD) process used to transport materials from a solid target onto a substrate, in a vacuum environment. To obtain the samples, the sputtering system generates a plasma from an inert gas. The positive ions of the plasma collide with the target and eject target atoms into space. Some of this atoms reach the substrate and start to condense, forming a tightly bound atomic layer. The thickness of the thin film will depend on the sputtering power, work pressure and deposition time [29]. Figure 2.18 shows a general diagram of a sputtering process, where the plasma is generated from Argon.

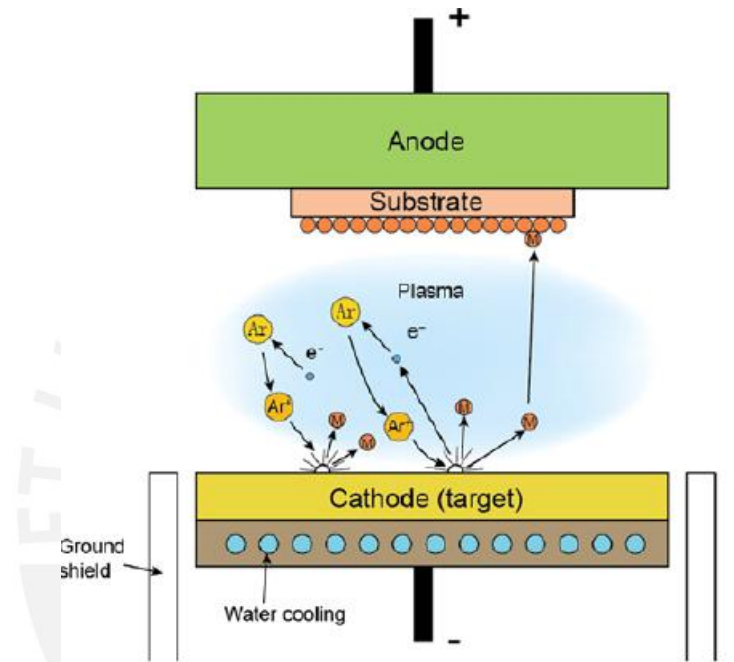


Figure 2.18: Diagram of a sputtering process. The positive ions of Argon plasma collide with the target and eject target atoms on the substrate [30].

2.5 Thermoelectric Elements

Thermoelectric or Peltier elements consist of multiple alternating n- and p-type semiconductors electrically connected in series between two ceramic plates [31], as shown in Figure 2.19. These elements are considered as heat pumps module which generate a temperature difference between its sides when a current is applied to it [32]. Three semiconductor principles are involved in the operation of thermoelectrical elements: Seebeck effect, Peltier effect and Thomson effect.

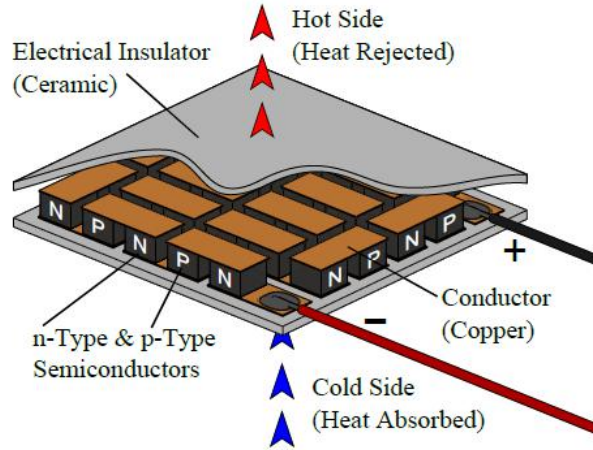


Figure 2.19: Peltier elements are comprised by n- and p-type semiconductors connected electrically in series. When current passes through the thermoelectric element, a temperature difference between its sides is generated [33].

The steady-state behavior of a thermoelectric element can be described by three equations [34]. Equation 2.29 represents the heat pumped at the cold side, Q_c , while, Equation 2.30 represents the heat rejected from the hot side, Q_h , where α is the Seebeck coefficient, R_m is the electrical resistance, K_m is the thermal conductance, I is the current, T_h is the temperature of the hot side and T_c is the temperature of the cold side.

$$Q_c = \alpha IT_c - \frac{1}{2}I^2 R_m - K_m(T_h - T_c) \quad (2.29)$$

$$Q_h = \alpha IT_h + \frac{1}{2}I^2 R_m - K_m(T_h - T_c) \quad (2.30)$$

Equation 2.31 shows that the voltage found at the terminal of the thermoelectric, V , depends on the current, I , and the temperature difference over the module.

$$V = \alpha(T_h - T_c) + IR_m \quad (2.31)$$

Seebeck Effect

Figure 2.20 shows two dissimilar conductors which are connected electrically in series but thermally in parallel. Thomas J. Seebeck experimentally found that when the junctions of the two dissimilar conductors are maintained at different temperatures, an electromotive force (emf), V , is developed in the open circuit [35]. The voltage V will depend on the temperature difference of the two junctions and a Seebeck coefficient, α , as shown in Equation 2.32.

$$V = \alpha(T_1 - T_2) \quad (2.32)$$

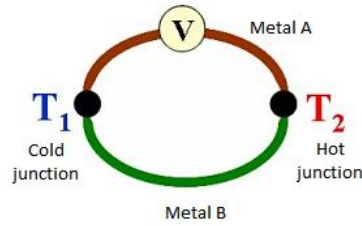


Figure 2.20: When the junctions of the two dissimilar conductors are maintained at different temperatures, an electromotive force, V , is developed in the open circuit.

Peltier Effect

Jean C.A. Peltier experimentally found that when an electrical current passes through a junction of two different conductors electrically in series and thermally in parallel, as shown in Figure 2.20, a rate of heating, q , is produced in one junction and a rate of cooling, $-q$, is produced in the other junction [35]. Both the generated and the absorbed heat depend on the current, I , and the Peltier coefficient, π , as shown in Equation 2.33.

$$q = \pi * I \quad (2.33)$$

Thomson Effect

William Thomson describes that the rate of generation of reversible heat, q , is proportional to the current that passes through a portion of a conductor and the temperature difference in the conductor portion [35], as shown in Equation 2.34, where, β , is the Thomson coefficient.

$$q = \beta * I * \Delta T \quad (2.34)$$

2.6 Control for temperature process

Temperature processes are very common in the industry. There are two basic controllers for this type of process: on-off controller and proportional–integral–derivative controller (PID). The correct choice of one of these controllers depends on the accuracy and the reliability that is needed during the process.

On-off controller

An on-off control is considered the simplest form to control a temperature process. It presents only two states: fully open or fully closed without any intermediate state. When the process variable (PV) is higher than the setpoint (SP), the controller output (CO) is fully open otherwise it is fully closed, as shown in Figure 2.21 A. In order to prevent damage to the process equipments due to rapid state changing (on-off), it is necessary to set a dead band that allows the temperature to exceed a certain value between the set point, as shown in Figure 2.21 B. On-off controllers are usually used when an accurate control is not needed and the temperature changes are very slowly [36].

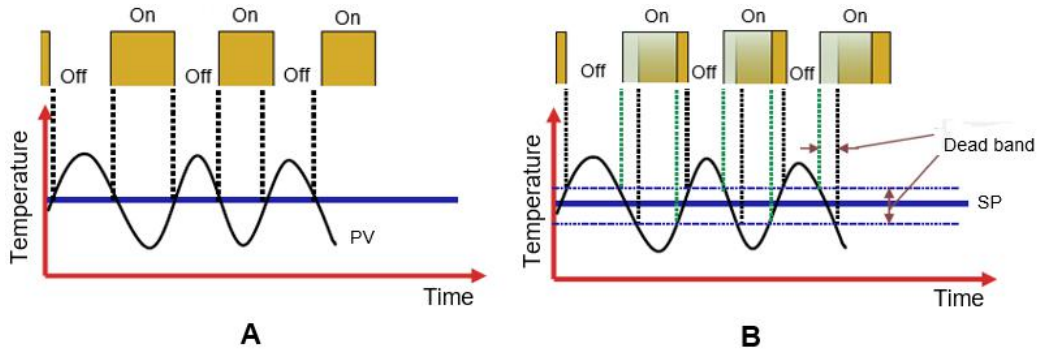


Figure 2.21: Part A. On-off controller for a temperature process
Part B. On-off controller with a dead band between the set point. [36]

PID controller

A proportional-integral-derivative (PID) control is the most popular algorithm employed in the industry due to the robust performance that presents a wide range of control system. This controller, shown in Equation 2.35, is comprising three coefficients: proportional K_p , integral T_i and derivative T_d that apply a correction to the error value $e(t)$ of a closed loop system [37].

$$u(t) = K_p[e(t) + \frac{1}{T_i} \int_t^0 e(t) d\tau + T_d \frac{de(t)}{dt}] \quad (2.35)$$

The proportional term provides a contribution which depends on the instantaneous value of the error. The proportional coefficient, referred as gain K_p , determines the ratio of output response to the error signal. On the other hand, the integral component takes into account the sum of the error value over time. The result implies a small error term that causes a slow increase in the controller output (CO). Finally, the derivative component acts on the rate of change of the control error and causes the output value (CO) to decrease if the process variable (PV) is increasing rapidly. The Derivative response is high sensitive to noise, therefore, it is not recommended to be used in fast processes because it can create instability in the control system [37]. Figure 2.22 shows the response of a PID controller for three different values of K_p .

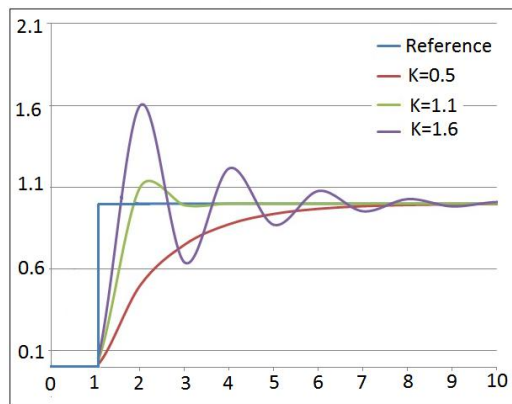


Figure 2.22: Response of a PID controller for three values of K_p .

Ziegler-Nichols method based on reaction curve

The Ziegler-Nichols reaction curve method is an empirical method of tuning a PID controller based on the transient response characteristics of the plant in open loop. Ziegler and Nichols proposed the following steps in order to determine the values of the proportional gain Kp , integral time Ti , and derivative time Td [37]:

- 1) With the plant in open loop at an initial time t_0 , apply a step change from u_0 to u_f in the range of 10 to 20 % of fully scale to the plant input.
- 2) Record the plant output until it stabilizes at a certain value, this curve is known as the process reaction curve.
- 3) Draw a tangent line at the inflection point of the curve, as shown in Figure 2.23 and calculate the parameters shown in Equations 2.36 2.37 2.38.

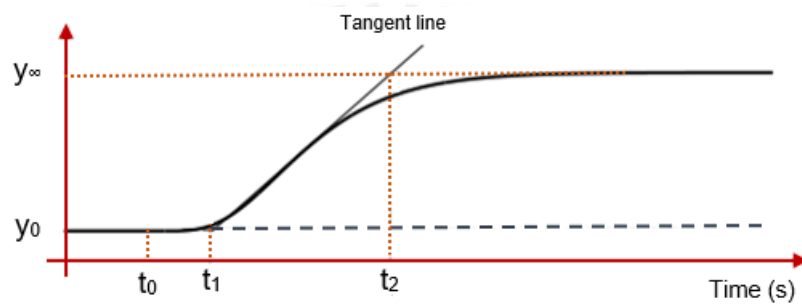


Figure 2.23: Plant reaction curve when a step change is applied in the plant input [37].

$$K_0 = \frac{y_f - y_0}{u_f - u_0} \quad (2.36)$$

$$\tau_0 = t_1 - t_0 \quad (2.37)$$

$$\nu_0 = t_2 - t_1 \quad (2.38)$$

- 5) Replace the parameter values in the equations shown in Table 2.2 to determine the values of Kp , Ti and Td .

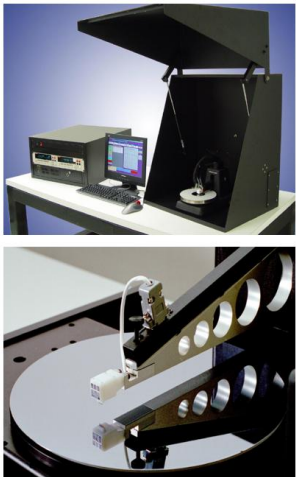

Table 2.2: Ziegler-Nichols PID controller tuning using the reaction curve method [37].

	Kp	Ti	Td
P	$\frac{\nu_0}{K_0 \tau_0}$	-	-
PI	$\frac{0.9\nu_0}{K_0 \tau_0}$	$3\tau_0$	-
PID	$\frac{1.2\nu_0}{K_0 \tau_0}$	$2\tau_0$	$0.5\tau_0$

2.7 Commercial designs of systems for resistivity measuring

Currently many resistivity measurement systems are available in the industry, some of them take into account the dependence of temperature on their measurements. A brief description of some of these designs are shown in Table 2.3.

Table 2.3: Commercial designs for resistivity measuring

Name	Description
<p>QuadPro Resistivity System</p> <p>Developed by Lucas Signatone Corporation</p>	<p>Allows measuring resistivity in samples of 10 to 300mm through a four point probes head. The probes are in line and equally spaced. The three available spacing between the probes are 0.04, 0.05 and 0.0625 inches. Tips are made of Tungsten Carbide. This system includes a computer, a stepper controller, a SourceMeter Keithley 2400, and optionally offers a thermal chuck system which provides temperatures of -55 to 600 °C. The software allows the selection of up to 49 points for automated testing and mapping of the test sample.</p>
	
<p>Model 680 Dynamic Four-Point Probe Sytem</p> <p>Developed by Four Dimensions Inc.</p>	<p>Allows measuring the resistivity of thin films on wafers up to 200mm in diameter in a temperature range of room temperature to 100 °C. Geometric corrections and repeatability tests are taken into account during the measures. Use a four point probes head fixed in a straight line. The probes are spaced 1mm among them. The software allows mapping the results in a 3D format.</p>
	

Chapter 3

Design and implementation of the measurement system

3.1 Description of the Hardware

The measuring system consists of a computer with LabVIEW software, five electrical measuring instruments by Keithley, a power supply PeakTech 1575, two connection boxes, a Peltier element, a thermocouple type K, a digital microscope camera and a GPIB-USB adapter. Figure 3.1 shows a full view of the measuring system.

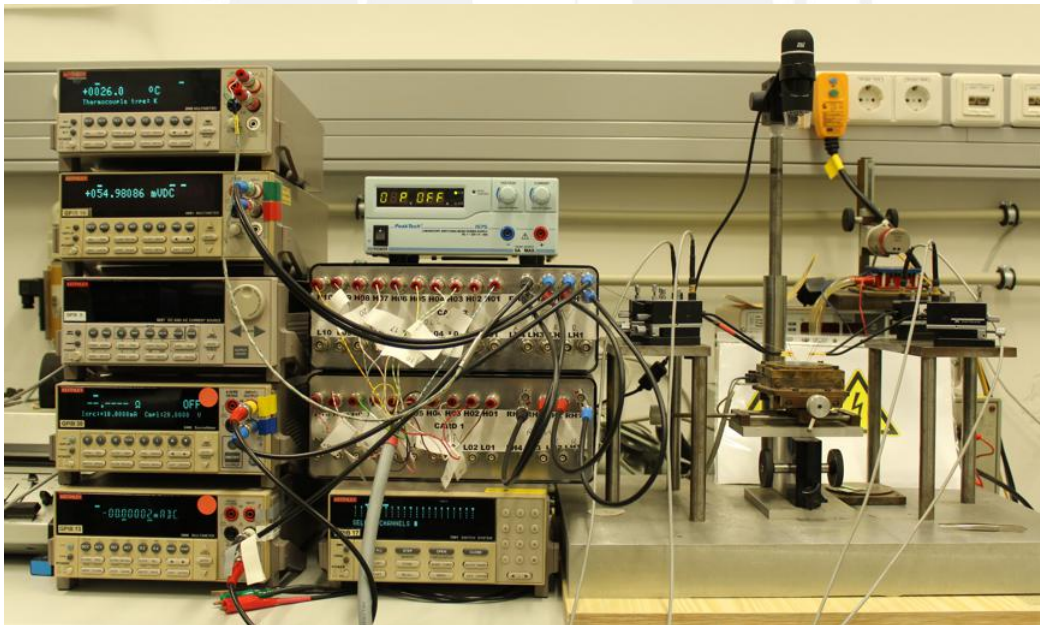


Figure 3.1: Full view of the measurement system.

Figure 3.2 shows the schematic diagram of system's hardware and the connections between each equipment. A LabVIEW program controls all the Keithley instruments, the PeakTech power supply, and the microscope camera. The NI GPIB USB HS+ adapter ensures the communication between the computer and the Keithley instruments. This adapter converts the serial bus of the computer into a general-purpose interface bus (GPIB) which is widely used in measuring and testing instruments.

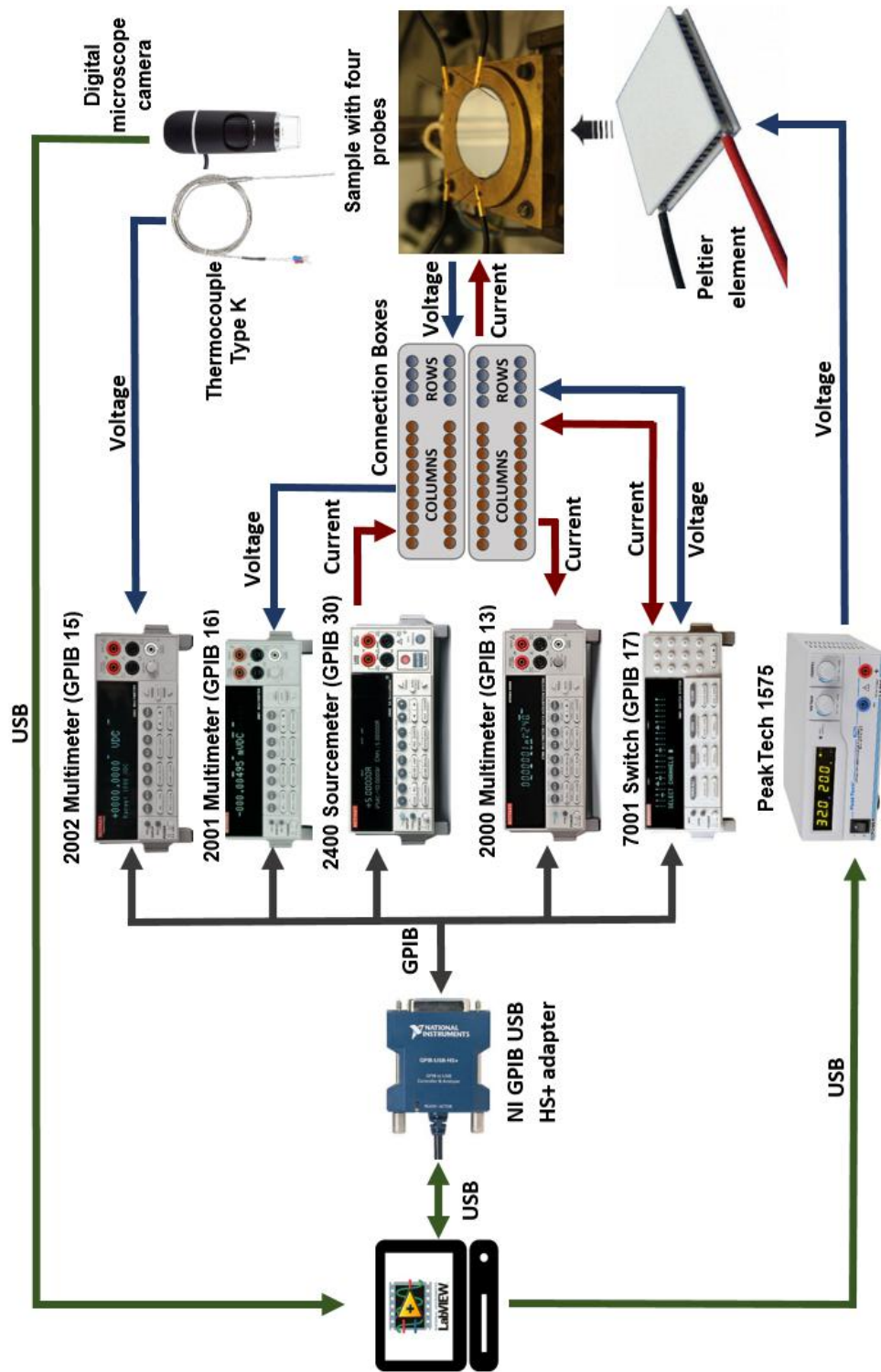


Figure 3.2: Schematic diagram of system's hardware. A LabVIEW program controls the Keithley instruments, a power supply PeakTech 1575 and a microscope camera. The corresponding GPIB addresses of the current setup are shown in brackets. The PeakTech 1575 provides different voltages to the Peltier element in order to change the temperature of the sample. [38–41]

The Keithley 2400 SourceMeter is used to send an electrical current through the two connection boxes at the sample, while the multimeters Keithley 2000 and Keithley 2001 are used to measure current and voltage in the sample, respectively. The two connection boxes were designed to join 40 channels and sort them into two arrays of 4 rows and 10 columns. For this measuring system, the fourth and first rows correspond to the current entering and leaving the sample, respectively, while the second and third rows measure the negative and positive voltage in the sample, respectively. Each column is connected to one probe in order to use the probes either for sourcing current or voltage measurement, as shown in Figure 3.3. Each connection box works with 4 probes. The switch equipment Keithley 7001 includes two cards with 40 channels each card, one card for each connection box, and is used to change automatically the pathway in the electrical circuits of the connection boxes. The system, furthermore, has a digital microscope camera that assists with the measurement of the distances between the probes in the corresponding method.

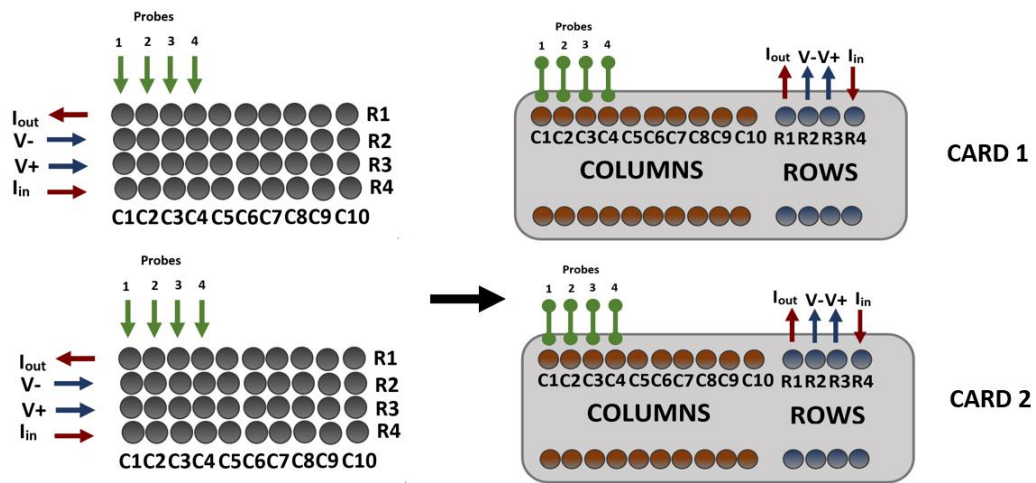


Figure 3.3: Switch channels are clustered and sorted into 2 arrays of 4 rows and 10 columns. Each column is a probe used either for sourcing current or voltage measurement.

In order to change the temperature of the sample during measurements, a Peltier element is used due to its thermoelectrical properties. A power supply PeakTech 1575, controlled by the computer via USB port, provides different voltages between 1 - 15 V DC to the Peltier element. Finally, a thermocouple type K is used to measure the temperature of the sample. A multimeter Keithley 2002 reads voltage generated by the thermocouple due to the difference between the temperature of the sample and the reference temperature and sends the electrical value in terms of temperature to the computer in order to use this information as a feedback for the control of the temperature in the sample.

A brief description of each equipment and component of the measuring system is provided in Table 3.1 and Table 3.2.

Table 3.1: Equipments of the measurement system









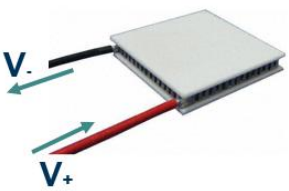

Instrument	Description
<p>Keithley 2400 SourceMeter (GPIB 30)</p> 	<p>This instrument provides high precision voltage and current with a 6 1/2 digit resolution. It also has an integrated multifunction of voltmeter and ammeter and works with a GPIB interface [38].</p>
<p>Keithley 2000 Multimeter (GPIB 13)</p> 	<p>Provides 6 1/2 digit resolution measurement with high speed and accuracy. Works with GPIB and RS-232 interfaces. It measures DC voltage from 100nV to 1000V and DC current until 3A. [39].</p>
<p>Keithley 2001 Multimeter (GPIB 16)</p> 	<p>Provides 7 1/2 digit resolution measurement with high speed and accuracy combined with a multiple measurement display and a GPIB interface. It measures DC voltage from 10nV to 1100V, DC current from 10pA to 2.1 A and thermocouple temperature from -200 °C to 1820 °C [42].</p>
<p>Keithley 2002 Multimeter (GPIB 15)</p> 	<p>Provides 8 1/2 digit resolution measurement with high speed and accuracy combined with a multiple measurement display and a GPIB interface. It measures DC voltage from 1nV to 1100V, DC current from 10pA to 2.1 A and thermocouple temperature from -200 °C to 1820 °C [43].</p>
<p>Keithley 7001 Switch System (GPIB 17)</p> 	<p>Keithley 7001 is a two-slot mainframe that switches signals from nanovolts to 1100V and femtoamps to 5A. Each slot supports 40 channels [40].</p>
<p>NI GPIB USB HS+</p> 	<p>NI GPIB USB HS+ is an adapter developed by National Instruments that transforms any USB port into a fully functional IEEE 488.2 controller for up to 14 programmable GPIB instruments. Transfers rates up to 1.8 MB/s.</p>

Table 3.2: Equipments of the measurement system (Continuation)

Instrument	Description
<p>Power supply PeakTech 1575</p> 	<p>The power supply PeakTech 1575 is a device which provides voltages between 1 to 32 VDC with a maximal current of 20 A. It is integrated with a 3 digits display and a USB 2.0 interface that gives the user the ability to control the voltage, current, period of time and cycles of the equipment via PC [41].</p>
<p>Digital microscope camera</p> 	<p>MicroCapturePro camera provided by DNT with 5 MP and led illuminator which works with a 2.0 USB interface, provides a high magnification.</p>
<p>Peltier element TEC1-12706</p> 	<p>This peltier element has a maximal temperature difference of 75 °C between its hot and cold faces when the hot side is maintained in 50 °C. It has a resistance of 2.1 Ω and supports 14.4 V or 6.4 A as maximal values. Its maximal operating temperature is 138 °C.</p>
<p>Thermocouple type K</p> 	<p>Thermocouple composed of two materials: chromel and constantan. It measures temperatures from -200 °C to 1260 °C with a sensitivity of approximately 41 $\mu\text{V}/^\circ\text{C}$. It presents a standard accuracy of +/- 2.2 °C.</p>

3.2 Preparation and description of the samples

For this thesis work, the thin film samples were prepared in the laboratories of the Institute of Micro and Nanotechnologies at the TU Ilmenau. A sputtering system LA 440S developed by Von Ardenne Anlagentechnik GMBH was used to obtain tungsten and aluminum thin film samples on silicon substrates of 2 inches in diameter. The thickness of the produced samples were 100, 300 and 600 nm. Figure 3.4 shows the sputtering system LA 440S and the obtained tungsten and aluminum thin films.

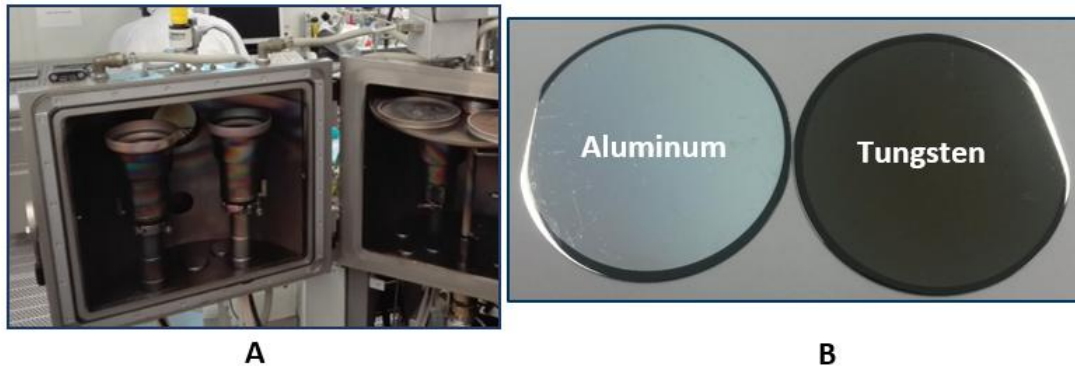


Figure 3.4: **A.** Sputtering system LA 440S developed by Von Ardenne Anlagentechnik GMBH **B.** Tungsten and aluminum thin film samples obtained with thickness of 100, 300, and 600 nm.

3.3 Temperature control

The temperature control in the sample is based on a PID algorithm. The Figure 3.5 shows the block diagram of the control system, where the temperature in the sample is acquired through a thermocouple type K. The multimeter Keithley 2002 reads the data from the thermocouple and send it to the PC in terms of temperature. This information is considered as the process variable, *PV*, and is compared to the desired temperature, *SP*, defined by the user in the program. The power supply PeakTech 1575 is the actuator that supplies different voltages to the Peltier element. The PeakTech 1575 voltages values depend on the PID controller developed in LabVIEW. A detailed information of the PID controller program is explained in "Description of the Software" section.

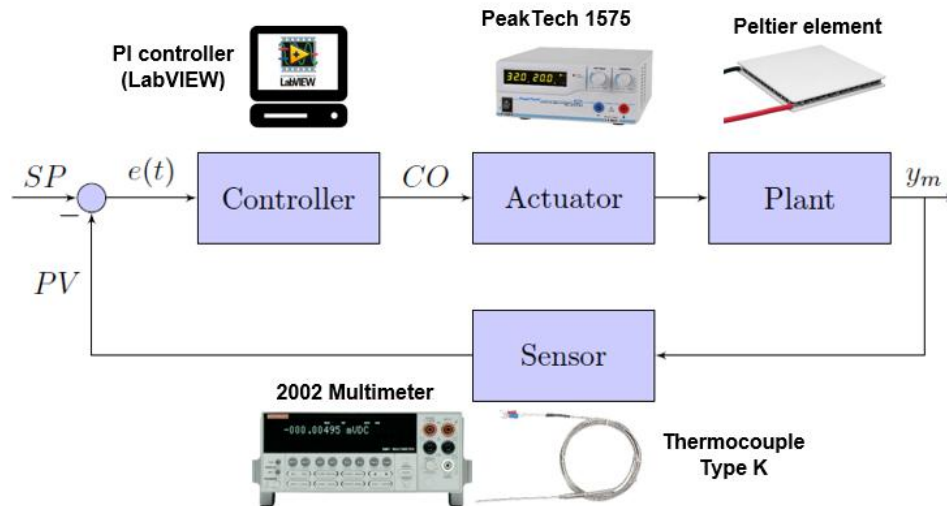


Figure 3.5: Block diagram of temperature control for the measuring system.

PID controller tuning

The PID controller coefficients were calculated according to Ziegler-Nichols method based on reaction curve. The first step is to determine the transient response of the Peltier element in an open loop. The transient response can be obtained from a mathematical model or an identified model. Mathematical models focused on a cooling operation of the Peltier element are available in the literature [44, 45]. However, for this work, it is necessary to find a model for a heating operation of the Peltier element.

MATLAB software offers tools for system identification and designing controllers. System Identification Toolbox provides MATLAB functions for constructing mathematical models of dynamic systems from measured input-output data. The Peltier element model was identified using this toolbox from the input-output data obtained. The figure 3.6 shows the response of Peltier element hot side when 3 V is supplied to its terminals and the identified model obtained from the measured data. According to the results, the identified model has a similitude of 94.6% regarding the measured response. Moreover, it can be observed that the identified dynamic model of the Peltier element has two poles and one zero, as shown in Equation 3.1

$$G(s) = 17.742 * \frac{1 + 97.748s}{(1 + 135.74s)(1 + 8.1349s)} \quad (3.1)$$

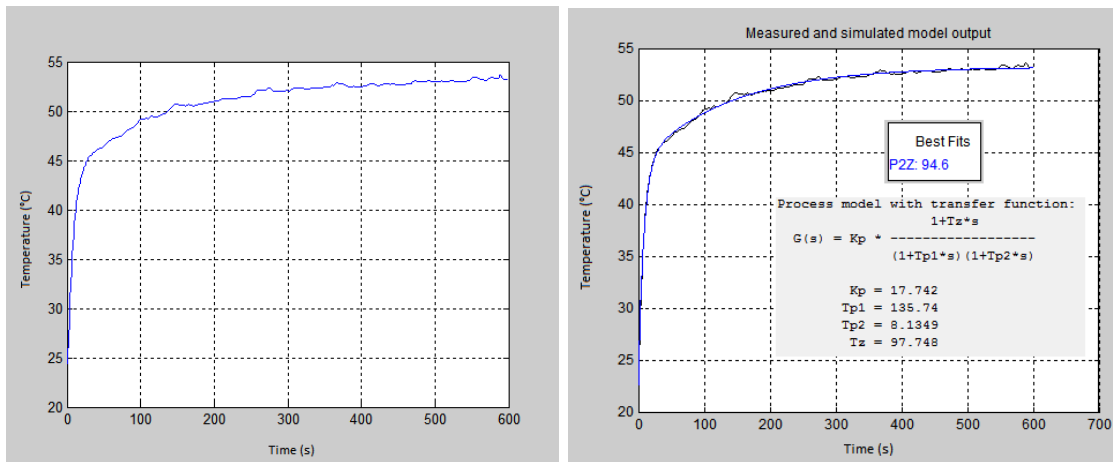


Figure 3.6: **A** Response of Peltier element hot side in an open loop when 4 V is supplied. **B** Identified model of the Peltier element using a System Identification Toolbox.

The Ziegler-Nichols parameters K_0 , τ_0 , and ν_0 are determined from the model, as shown in Figure 3.7. The PID coefficients are calculated replacing the parameter in equations, shown in Table 2.2. The results are: $K_p = 0.15$, $T_i = 0.015$, and $T_d = 0.003$.

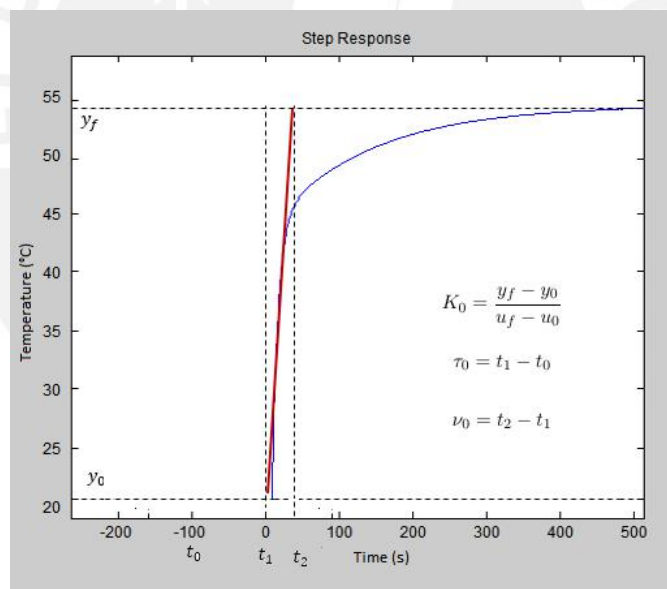


Figure 3.7: Ziegler-Nichols parameters K_0 , τ_0 , and ν_0 are determined from the identified model.

The PID controller coefficients can be also determined using the Control System Toolbox provided by MATLAB. This Toolbox allows to analyze and design the PID controllers for a given model. Figure 3.8 shows the PID coefficients obtained from the identified transfer function. Furthermore, it is shown the rise time and the response time of the measuring system.

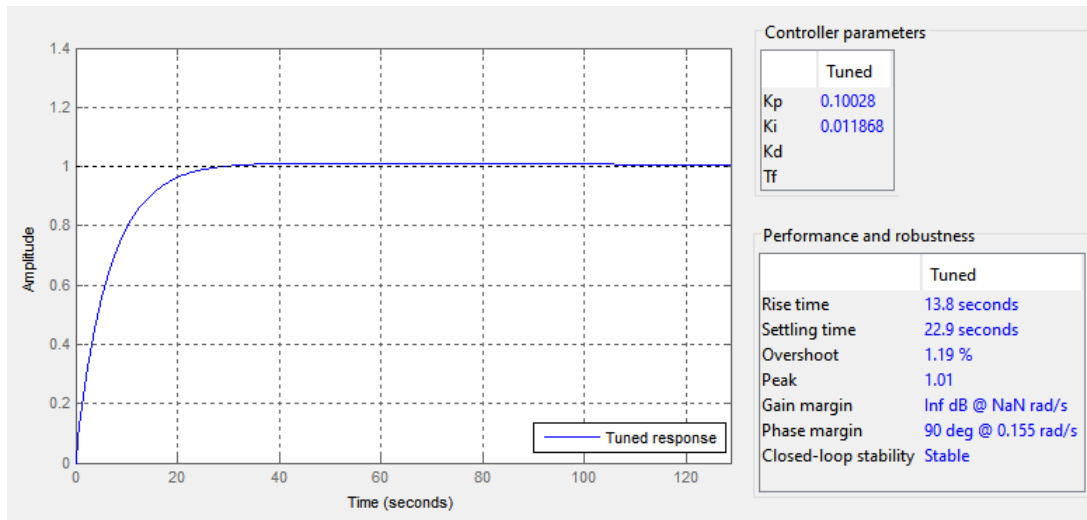


Figure 3.8: PID controller tuning using MATLAB Control System Toolbox.

In order to verify how is the behavior of the measuring system, it was implemented an auxiliary program that allows entering the PID coefficients already calculated and measure the response time. The auxiliary program is shown in Figure 3.9.

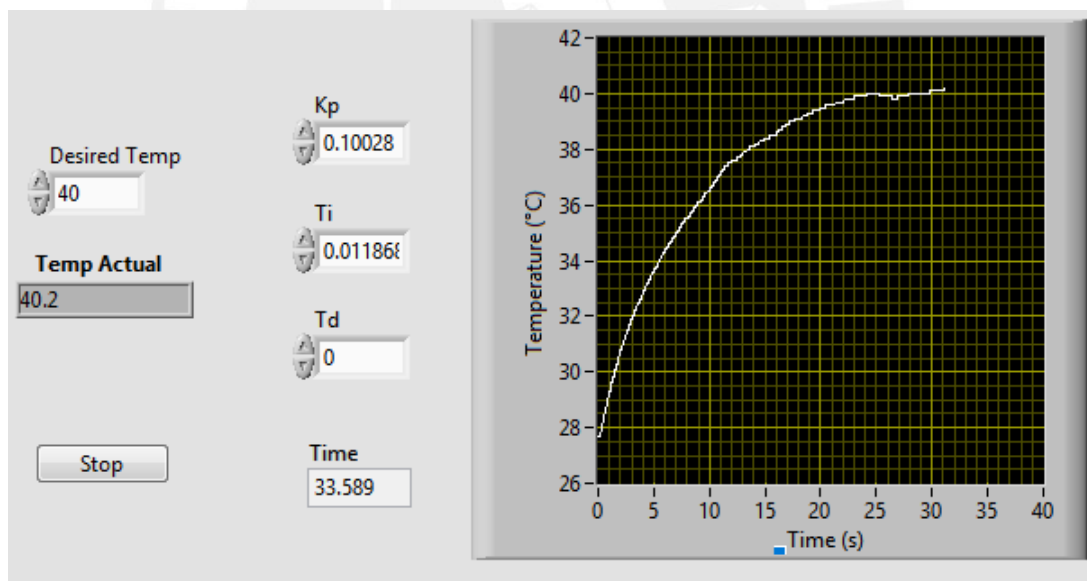


Figure 3.9: Auxiliary program to verify how is the behavior of the measuring system with the calculated PID coefficients.

The results shows that the rise time of the measuring system is approximately 14 s and the response time is 25 s. Table 3.3 shows that the rise time and the response time values determined by the Toolbox are similar to the time values measured in the auxiliary program.

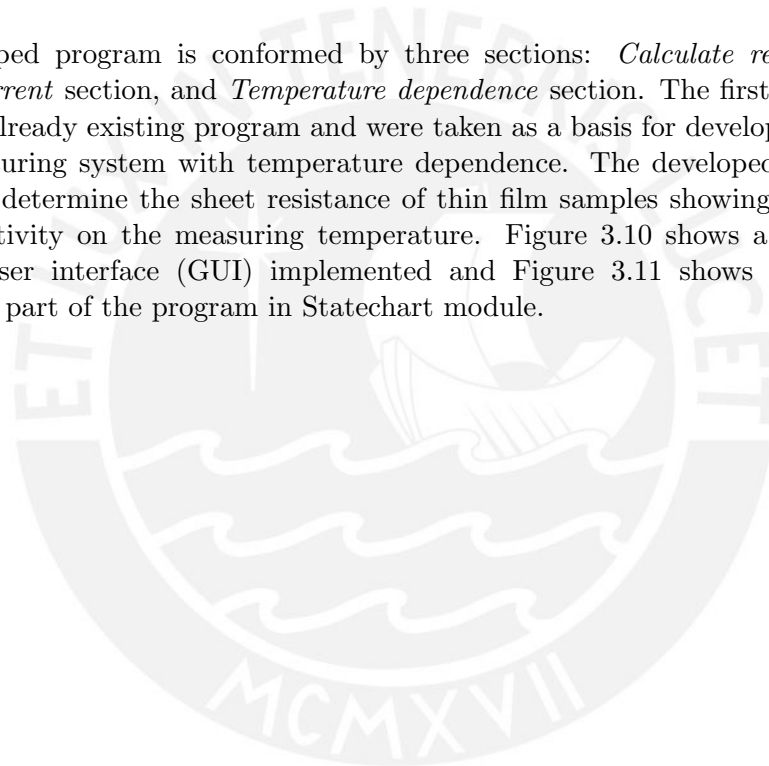
Table 3.3: Rise time and response time values.

	Rise time (s)	Response time (s)
PID tuning Toolbox values	13.80	22.90
Measured values	14.00	25.00

3.4 Description of the Software

The software for the measuring system was developed with the graphical programming software LabVIEW that provides characteristics for communicating and controlling the measuring system's hardware. Statechart, a state-based programming LabVIEW module, was used to structure the logic of the program. This LabVIEW module provides features for designing sequential applications between transitions and events.

The developed program is conformed by three sections: *Calculate resistivity* section, *Voltage-Current* section, and *Temperature dependence* section. The first two sections are part of an already existing program and were taken as a basis for developing the software of the measuring system with temperature dependence. The developed software allows the user to determine the sheet resistance of thin film samples showing the dependency of the resistivity on the measuring temperature. Figure 3.10 shows a full view of the graphical user interface (GUI) implemented and Figure 3.11 shows the temperature dependence part of the program in Statechart module.



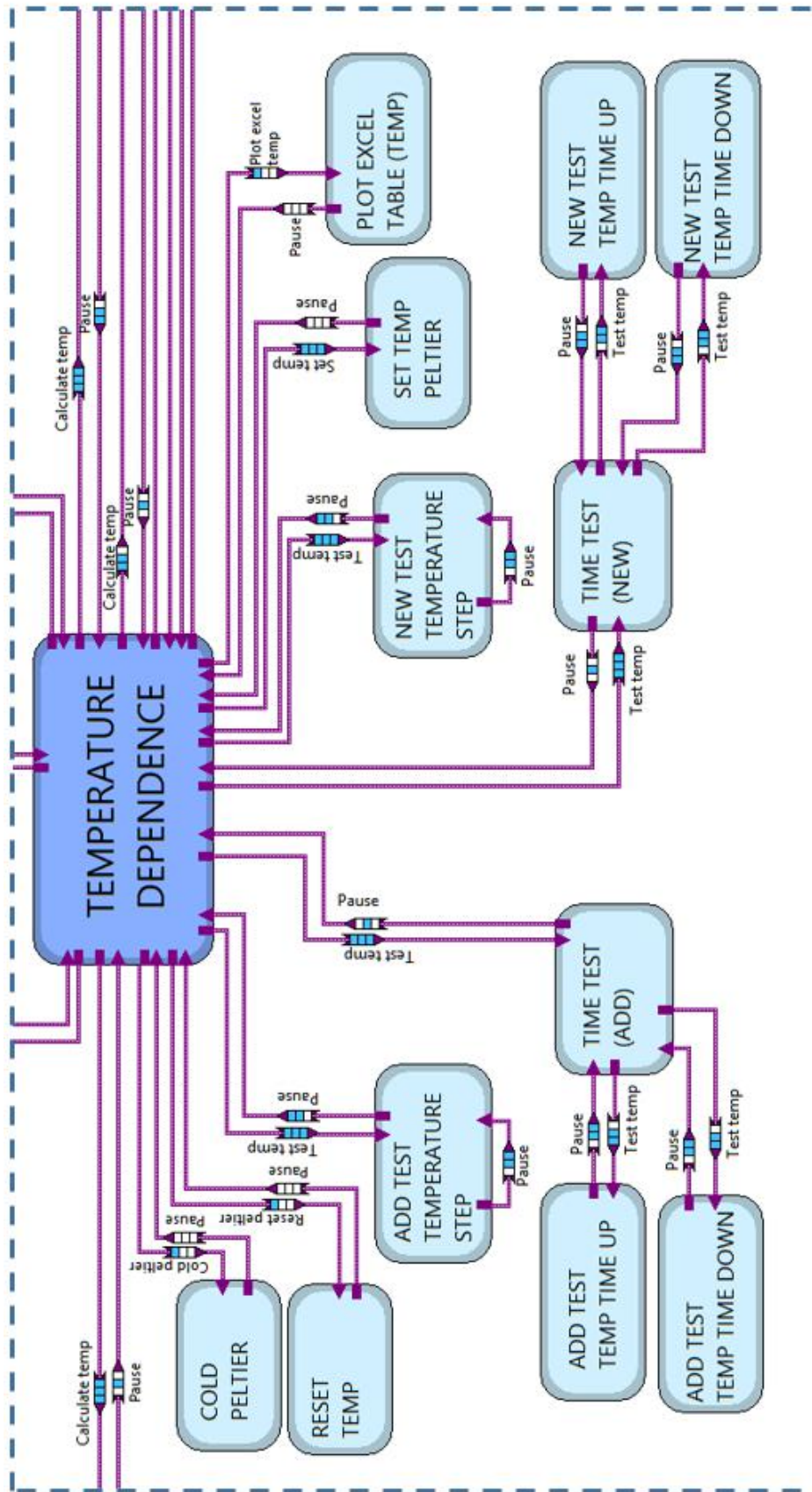


Figure 3.11: Sequential events of temperature dependence part in Statechart module.

Calculate resistivity section

The *Calculate resistivity* section allows the user to choose among four electrical resistivity measuring methods (Van der Pauw, Modified Van der Pauw, Linear Van der Pauw and Linear Four Probes). Every method has its own characteristics and procedure, therefore, the user must follow different steps in this section before starting the measurement. A detailed explanation of the steps to follow in each method is described below. Figure 3.12 shows a full view of *Calculate resistivity* section.

Voltage-Current section

The *Voltage-Current* section allows to plot a Current-Voltage curve when a current is applied to the sample. The system measures the voltage and current in the probes and shows these values in a graph. The results are shown in a table and can be exported to an Excel file. A full view of *Voltage-Current* section is shown in Figure 3.13.



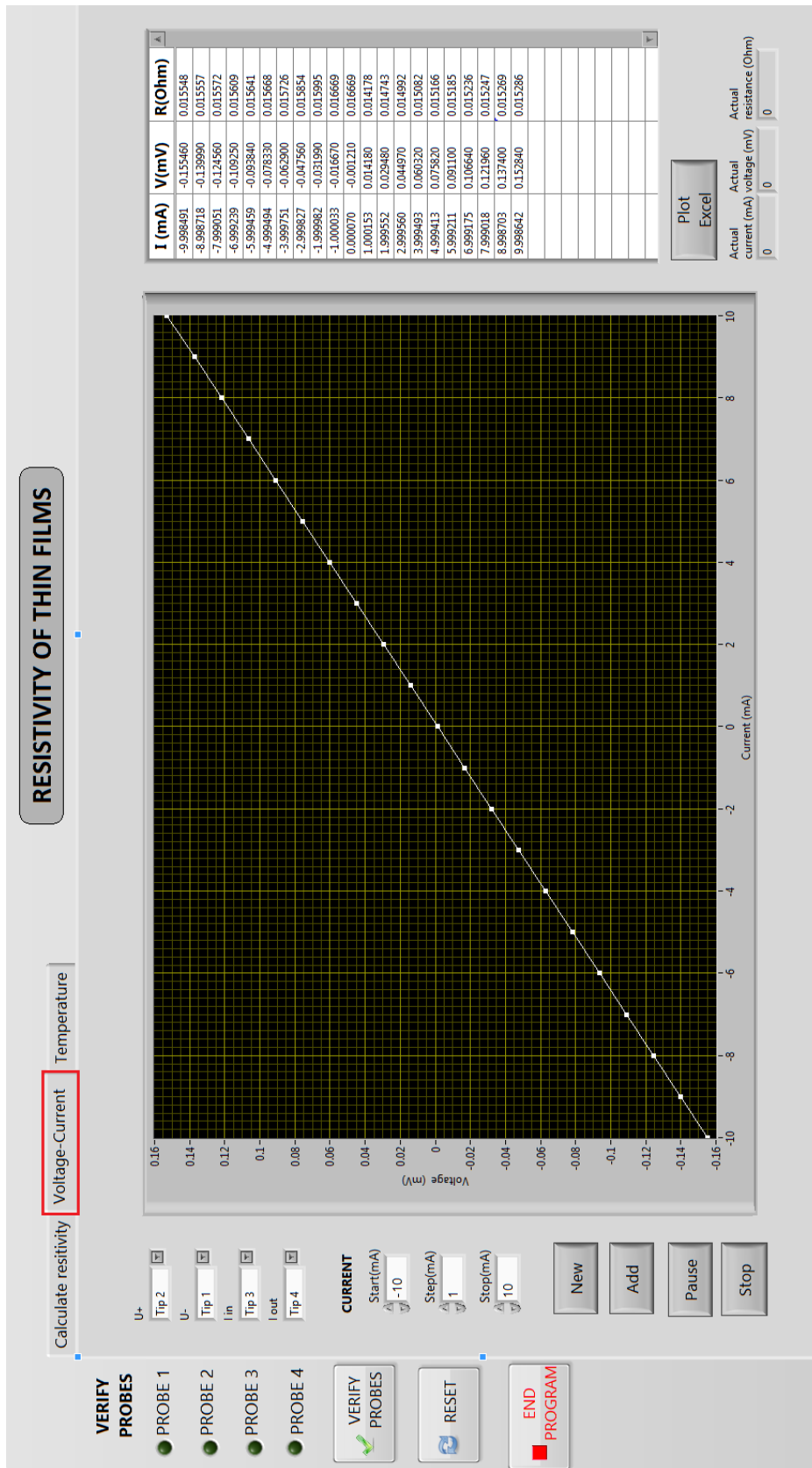


Figure 3.13: GUI of Voltage-Current section.

Temperature dependence section

The temperature dependence section was implemented into the already existing system. This section allows to determine the sheet resistance of thin film samples showing the dependency of the resistivity on the measuring temperature. The resistivity measurements in this section can be performed giving two alternatives: measurements with fixed temperature and measurements with variable temperature.

Measure with Fixed Temperature

The *Measure with Fixed Temperature* alternative allows the user to set the temperature of the sample at a particular value before carrying out the measurements. The desired temperature is entered in the box *Set Temperature* and established pressing check button next to *Set Temperature* box. *Actual Temperature* box gives an information of the sample temperature measured by the thermocouple type K, as shown in Figure 3.14.

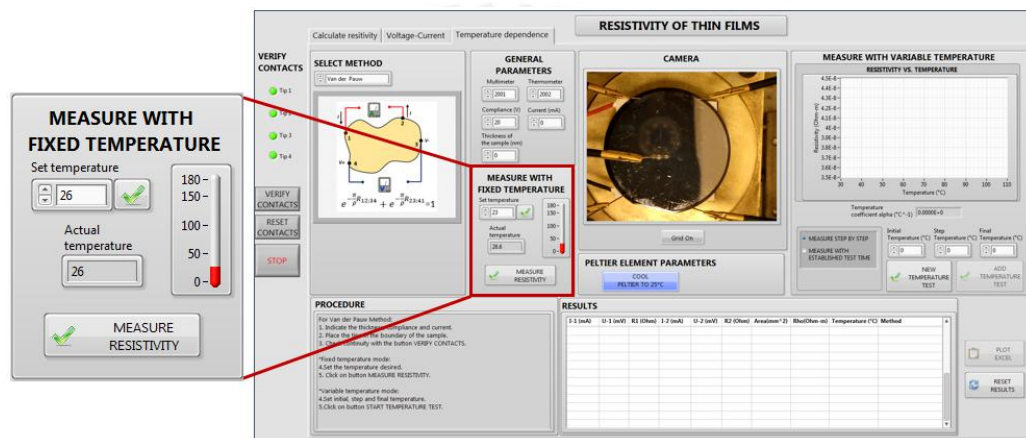


Figure 3.14: GUI of the measuring system developed with LabVIEW - Measure with Fixed Temperature section.

When the check button is pressed, a dialog window will appear showing a message with the desired temperature and a thermometer with the actual temperature of the sample, as shown in Figure 3.15. The dialog window will automatically disappear when the temperature of the sample reaches the desired temperature.

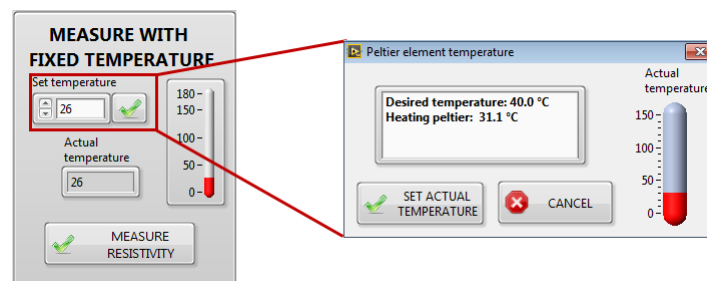


Figure 3.15: Measure with Fixed Temperature section - a dialog window appears showing a message with the desired temperature and a thermometer with the actual temperature.

A PID controller was implemented to set the temperature of the sample at a particular value. The LabVIEW program of the controller is shown in Figure 3.16.

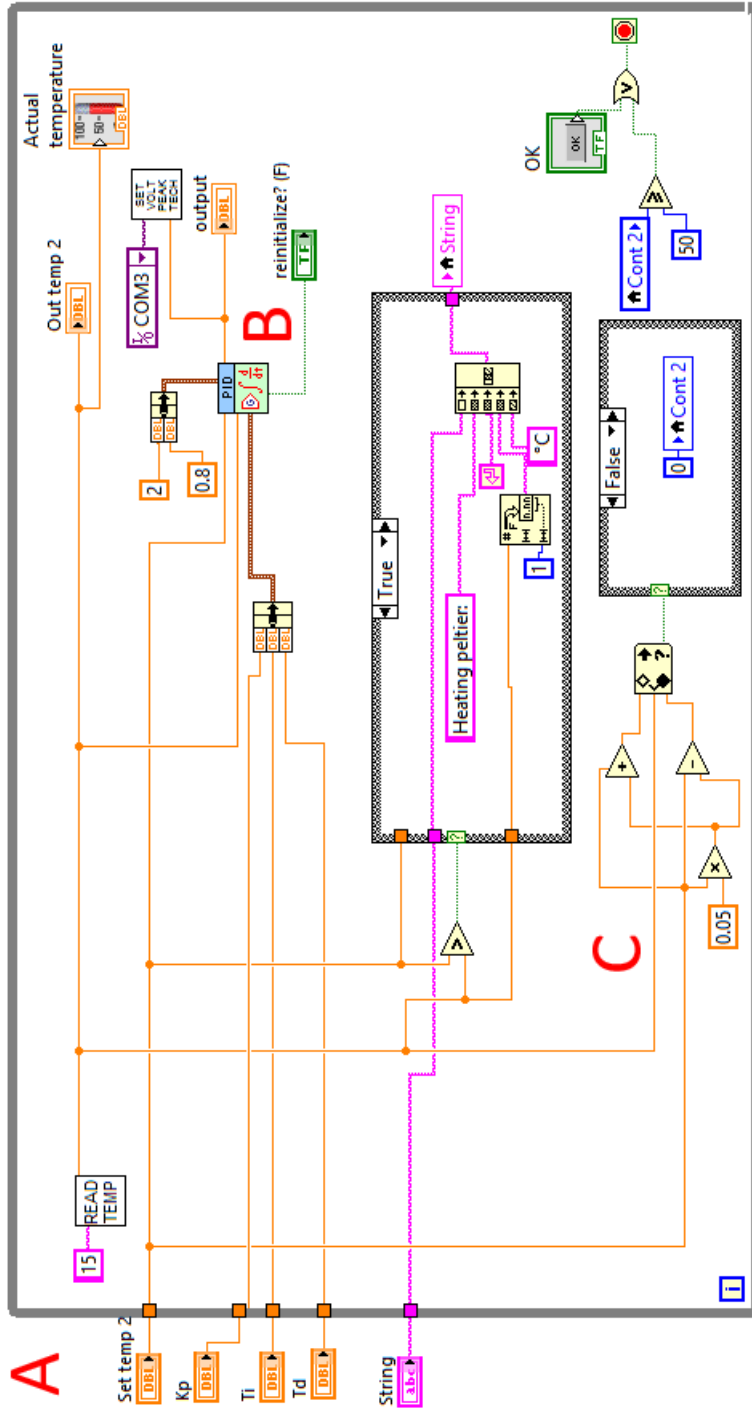


Figure 3.16: Measure with Fixed Temperature - LabVIEW programming of PID controller.

- A. Set point and process variable are read from the GUI.
- B. The PID algorithm controls the power supply PeakTech 1575 according to the PID coefficients.
- C. The control ends when the process variable reaches the set point with a tolerance of 1%. This tolerance can be changed in the program.

The steps to follow in the GUI in order to realize the resistivity measurements are shown in Figure 3.17.

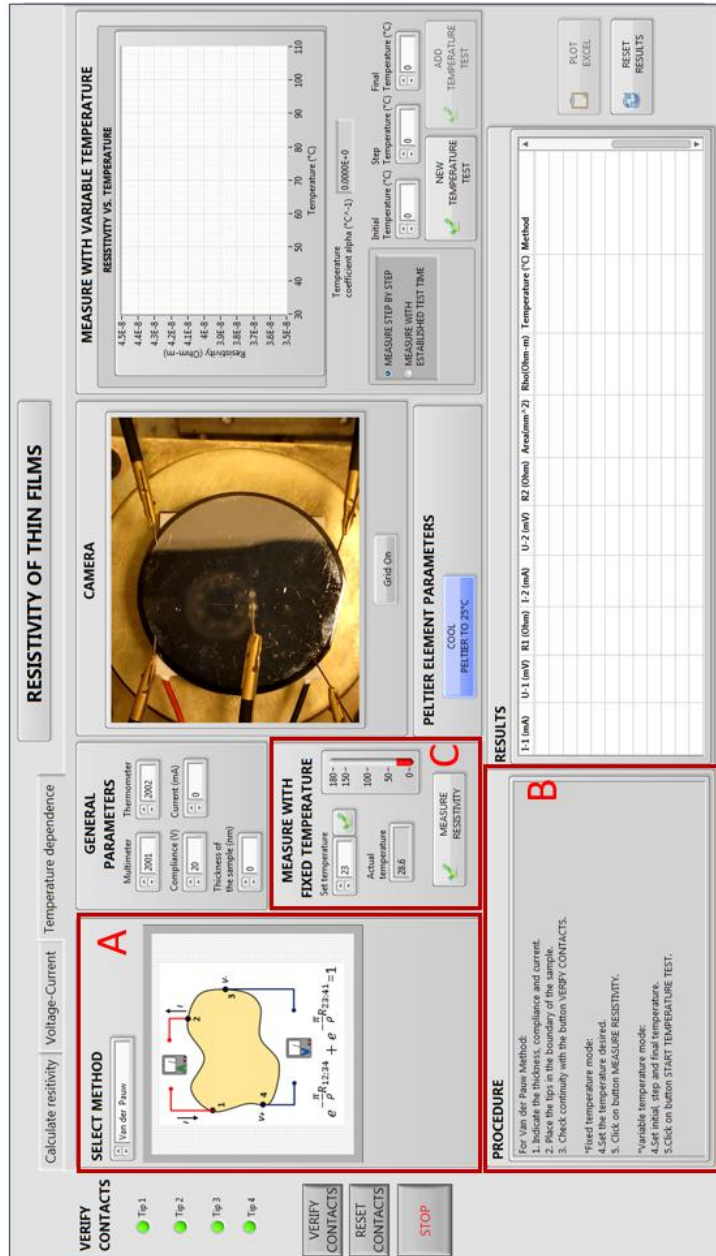


Figure 3.17: Resistivity measuring with fixed temperature.

- A. Select a resistivity measuring method in *CALCULATE RESISTIVITY* section. The selected method will appear in *SELECT METHOD* area.
- B. According to the chosen method, follow all the procedures before the measuring in *CALCULATE RESISTIVITY* section. The procedure is also shown in *PROCEDURE* area.
- C. Set the temperature to the sample at a particular value and measure the electrical resistivity pressing *MEASURE RESISTIVITY* button in *MEASURE WITH FIXED TEMPERATURE* section.

Measure with Fixed Temperature

The *measurements with variable temperature* alternative consists in the step of selecting among the four resistivity measuring methods and following the corresponding procedure before the measurement in *Calculate resistivity* section. The second step is the definition of the initial, step and final temperatures in *Temperature dependence* section, as shown in Figure 3.18.

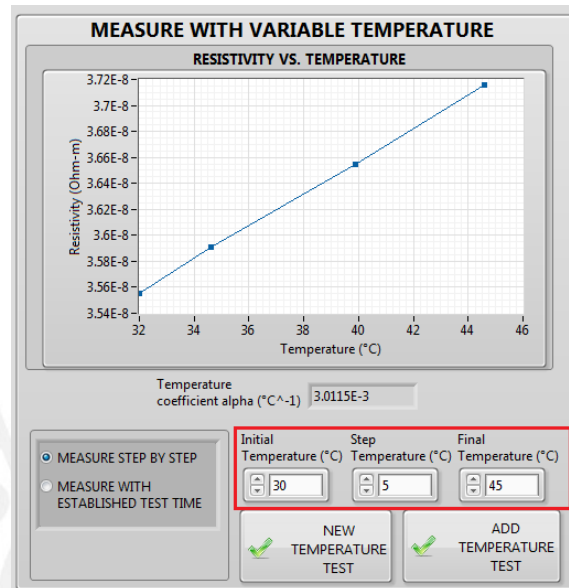


Figure 3.18: Measure with Variable Temperature section - definition of the initial, step and final temperatures.

Two types of measuring can be chosen in this alternative: *step by step measuring* or *measuring during a set time*, as shown in Figure 3.19.

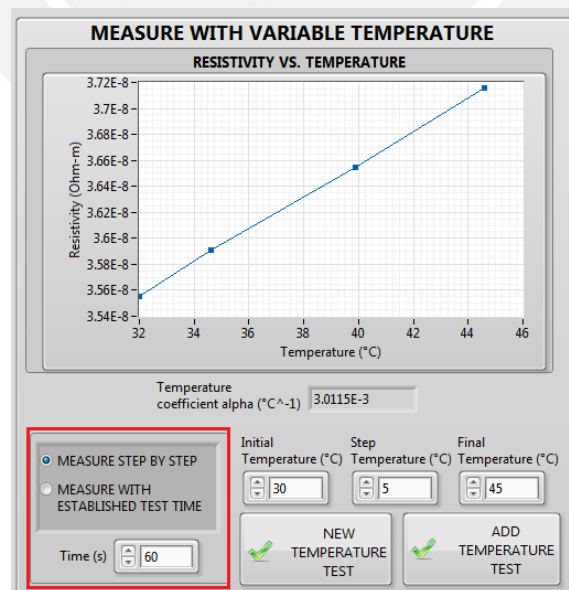


Figure 3.19: Types of measuring in *Measure with Variable Temperature* alternative.

The *Step by step measuring* option will heat the sample until the temperature reaches a step temperature and automatically will measure the sample's resistivity. This process will be repeated until reaching the final temperature. On the other hand, *Measuring during a set time* option will heat the sample until the final temperature during a time set by the user and will measure automatically the sample's resistivity each time a step temperature is reached. The minimum set time will depend on the Peltier element response in time. For the model TEC1-12706 the minimum time that can be set is 60 seconds.

The graphic placed at the upper right corner of the GUI will plot the results as Temperature vs. Resistivity. Furthermore, the temperature coefficient of the results will appear below the graphic, as shown in Figure 3.20.

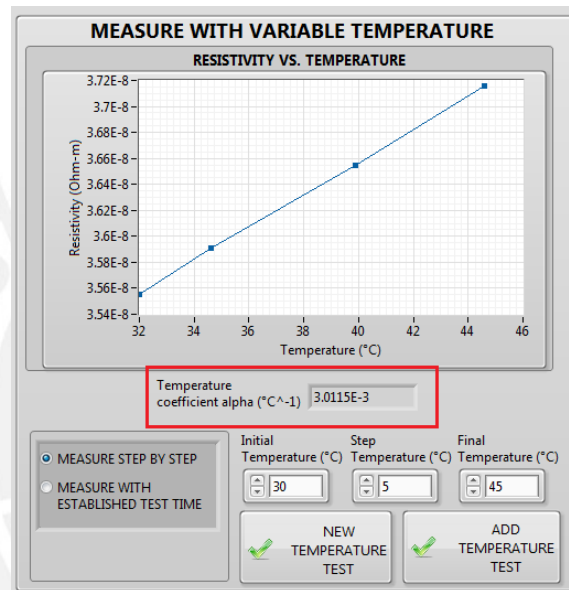


Figure 3.20: The temperature coefficient of the results.

A detail explanation of the steps that should be followed during the measurement procedure using the GUI is shown in Figure 3.21.

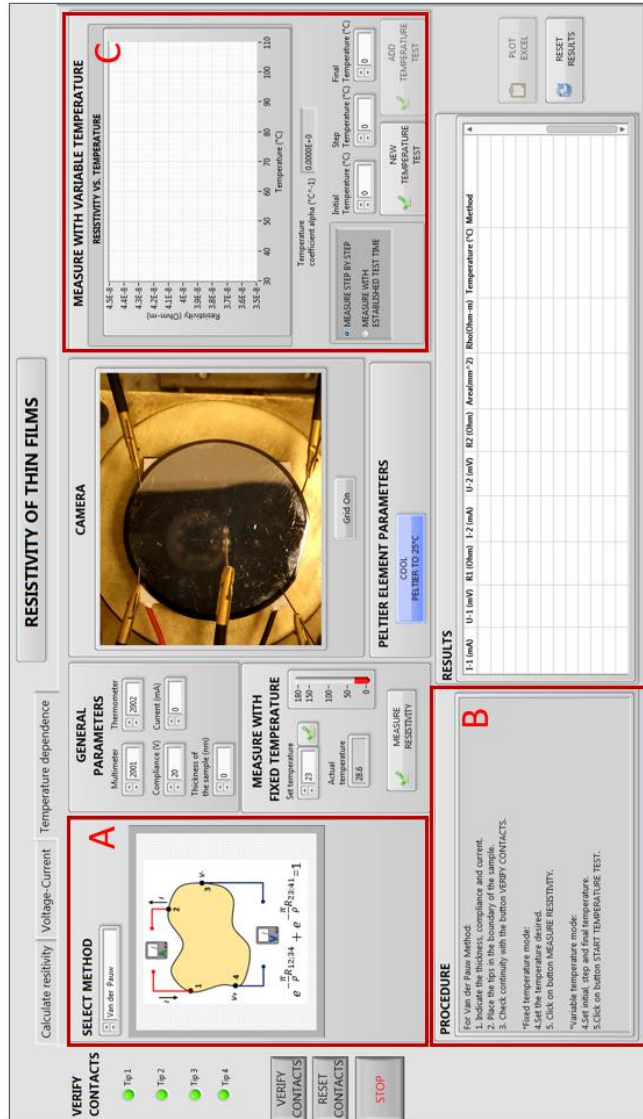


Figure 3.21: Resistivity measuring with variable temperature.

- A. Select a resistivity measuring method in *CALCULATE RESISTIVITY* section. The selected method will appear in *SELECT METHOD* section.
- B. According to the chosen method, follow all the procedures before the measuring in *PROCEDURE* section. The procedure is also shown in *PROCEDURE* area.
- C. Set the initial, step and final temperatures values in *MEASURE WITH VARIABLE TEMPERATURE* section.
 - C1. Choose between two measuring types: *step by step* or *during a set time* and measure the electrical resistivity pressing *START TEMPERATURE TEST* button in *MEASURE WITH VARIABLE TEMPERATURE* section. In case to choose *measuring during a set time* option a input box will appear to set the test time the in seconds.

The GUI of *Temperature dependence* section shows an image of the sample with the four probes and the thermocouple tip. Some of the methods require an image measurement system that is accomplished using the camera. The measurement results are shown in the table placed on the bottom right side of the GUI. The results can be exported to an Excel file. A detail explanation of every sector considering some important parts of the programming is described as follows:

Verify Contacts

In order to avoid electrical discontinuity errors between the probes and the sample during the measurements, *Verify Contacts* area allows verifying the continuity of the contacts at every time the user considers appropriate. The continuity verification initializes pressing the button *VERIFY CONTACTS*, as shown in Figure 3.22. There are 4 LEDs corresponding to every probe and they are lighted when the continuity in each probe is checked. The continuity in a probe is checked when the differences between the current measurements in the probe and the current applied to the other probes are less than 30%. Figure 3.23 shows the LabVIEW program designed for Verify Contacts area.



Figure 3.22: GUI of the measuring system developed with LabVIEW. Verify contacts area.

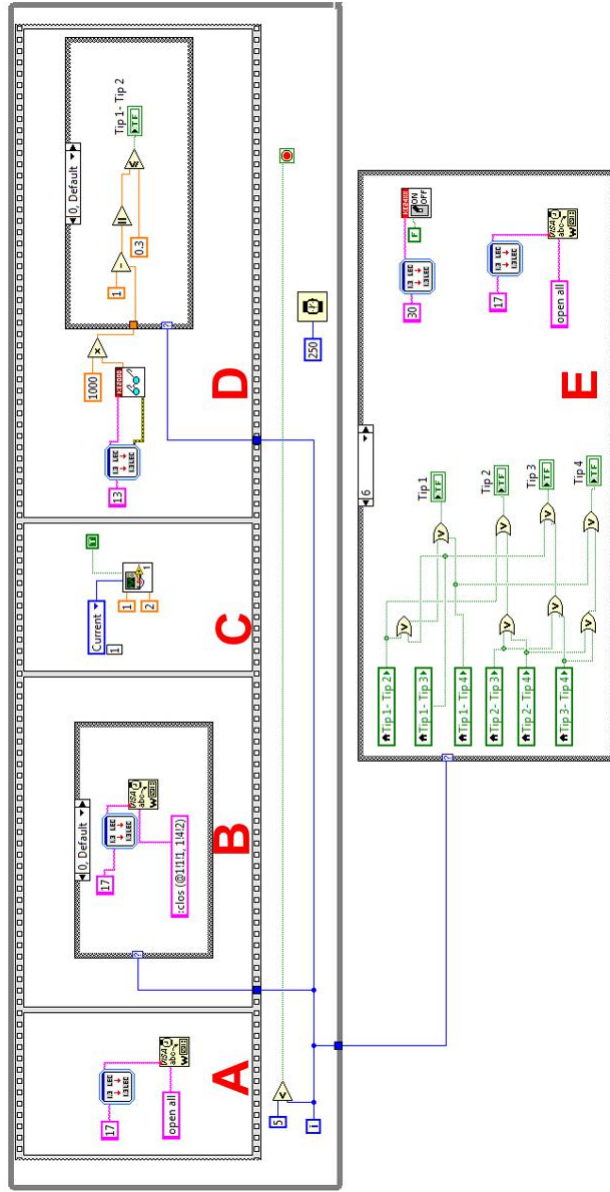


Figure 3.23: Verify Contacts area - LabVIEW programming.

- A. The channels in the switch equipment are opened. Therefore, there are no electrical connections between the contacts.
- B. The channels are closed sequentially between every pair of probes.
- C. A current of 1 mA is applied by the SourceMeter Keithley 2400 between these pair of probes.
- D. The current between these pair of probes is measured and the LED will be lighted when the difference between the value of the applied and measured current is less than 30 %. This value can be modified in the program.
- E. A logic configuration is set to determine exactly which probe has or does not electrical continuity.

General Parameters

Resistivity measuring methods implemented in the system require determining the sheet resistance of thin film samples. Therefore, the SourceMeter Keithley 2400 supplies a current flow through the sample. The value of this current is set in the box *Current (mA)* of General Parameters sector, as shown in Figure 3.24. Moreover, when sourcing current, the SourceMeter Keithley 2400 can be set to a safety limited voltage for the test. This limit voltage is known as compliance and in the GUI can be limit in the box *Compliance(V)* among 2, 20 or 200 V. The correct choice of the Compliance value will depend on the sheet resistance in order to define the maximum current that can pass through the sample. *Multimeter* and *Thermometer* boxes allows the user to define which type of Keithley multimeter will perform the function of voltmeter and thermometer, respectively

On the other hand, the thickness of the sample is an information considered in the calculation of the resistivity and should be entered in the box *Thickness of the sample(nm)*.

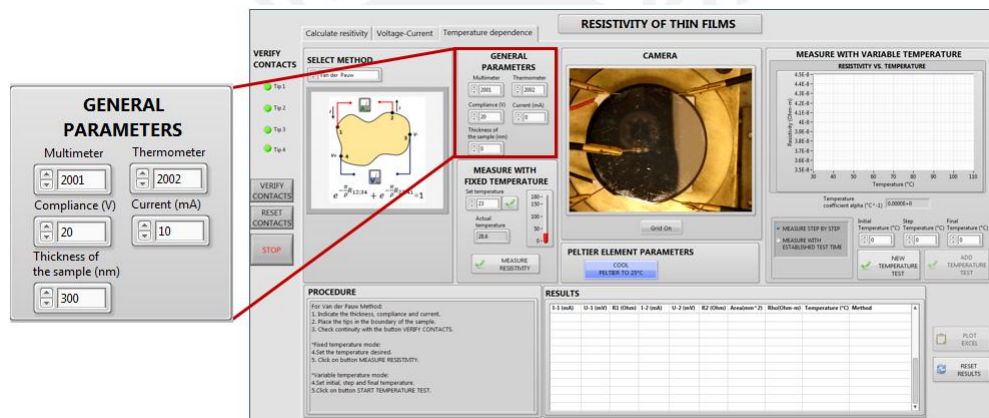


Figure 3.24: GUI of the measuring system developed with LabVIEW - General Parameters area.

Camera

The configuration of the four probes on the sample depends on the selected resistivity measuring method. *Camera* area shows continuously an image of the sample and assists in the positioning of the probes. When *Grid on* button is pressed, a mesh on the image is created, as shown in Figure 3.25. *Grid off* button turns off the mesh. The mesh on the image improves the positioning accuracy of the tips during the measurements.

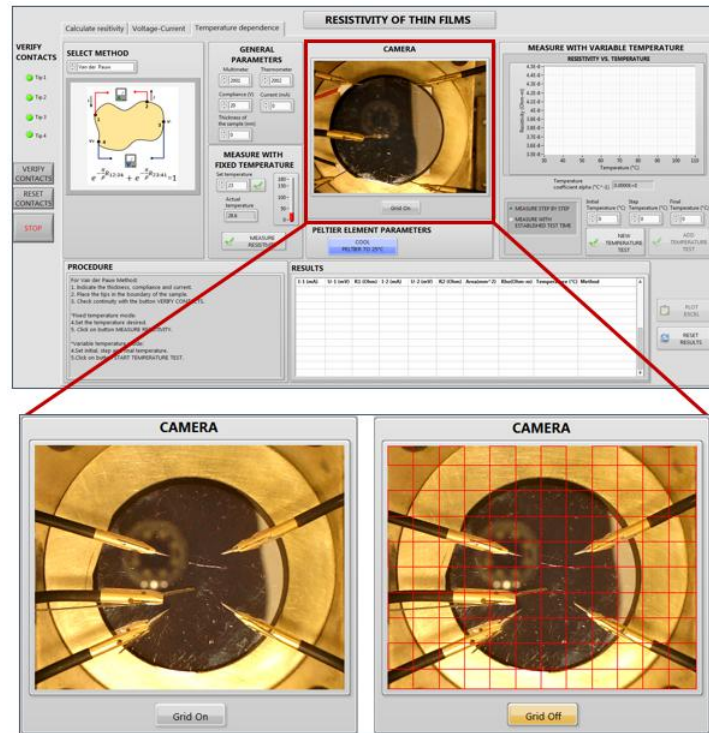


Figure 3.25: GUI of the measuring system developed with LabVIEW - Camera area.

Select Method

Select method area shows the selected method in *Calculate resistivity* section, as shown in Figure 3.26. Every method has its own procedure, therefore, depending on the selection the user must follow different steps. The procedure and some important parts of the LabVIEW program of each method are described below.

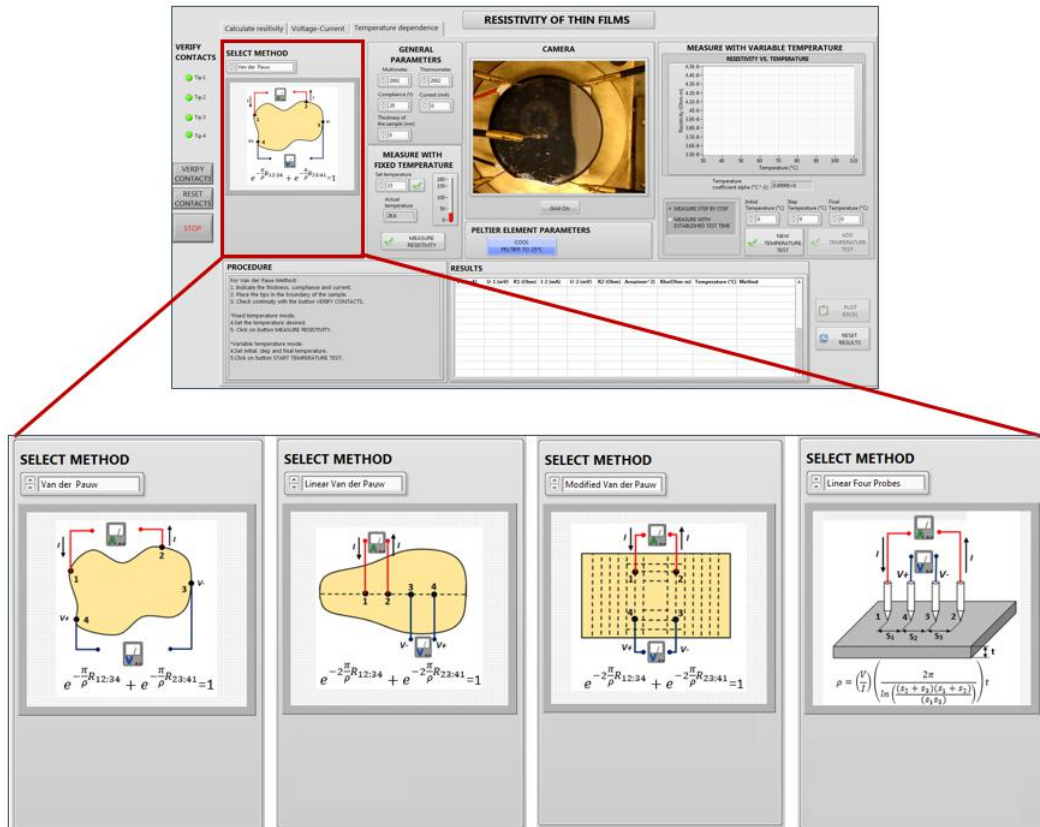


Figure 3.26: GUI of the measuring system developed with LabVIEW - Select Method area.

Measure with Van der Pauw method

When Van der Pauw method is selected, an image with the schematic, probes configuration and equation of the method appears in the GUI, as shown in Figure 3.27.

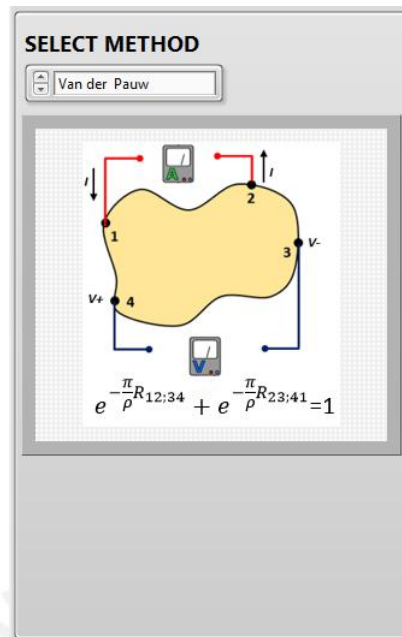


Figure 3.27: Van der Pauw method - schematic, equation and probes configuration.

The procedure to measure the electrical resistivity with this method in the GUI is as follows:

Steps in Calculate resistivity section:

1. Choose Van der Pauw method
2. Place the probes on the boundaries of the sample.
3. Check continuity with the button *VERIFY CONTACTS*.

Steps in Temperature dependence section:

4. Indicate the thickness of the sample, the current and the voltage compliance for the test in *General Parameters* section.

• **Fixed Temperature mode:**

5. Set the temperature as desired and click on the button check in *Measure with Fixed Temperature* section.

6. Click on button *MEASURE RESISTIVITY*.

• **Variable Temperature mode:**

5. Set initial, step and final temperatures in *Measure with Variable Temperature* section.

6. Choose between *step by step measuring* or *measuring during a set time* in *Measure with Variable Temperature* section.

7. Click on button *START TEMPERATURE TEST*.

A brief description of the Van der Pauw program sequenced by capital letters is shown in Figure 3.28.

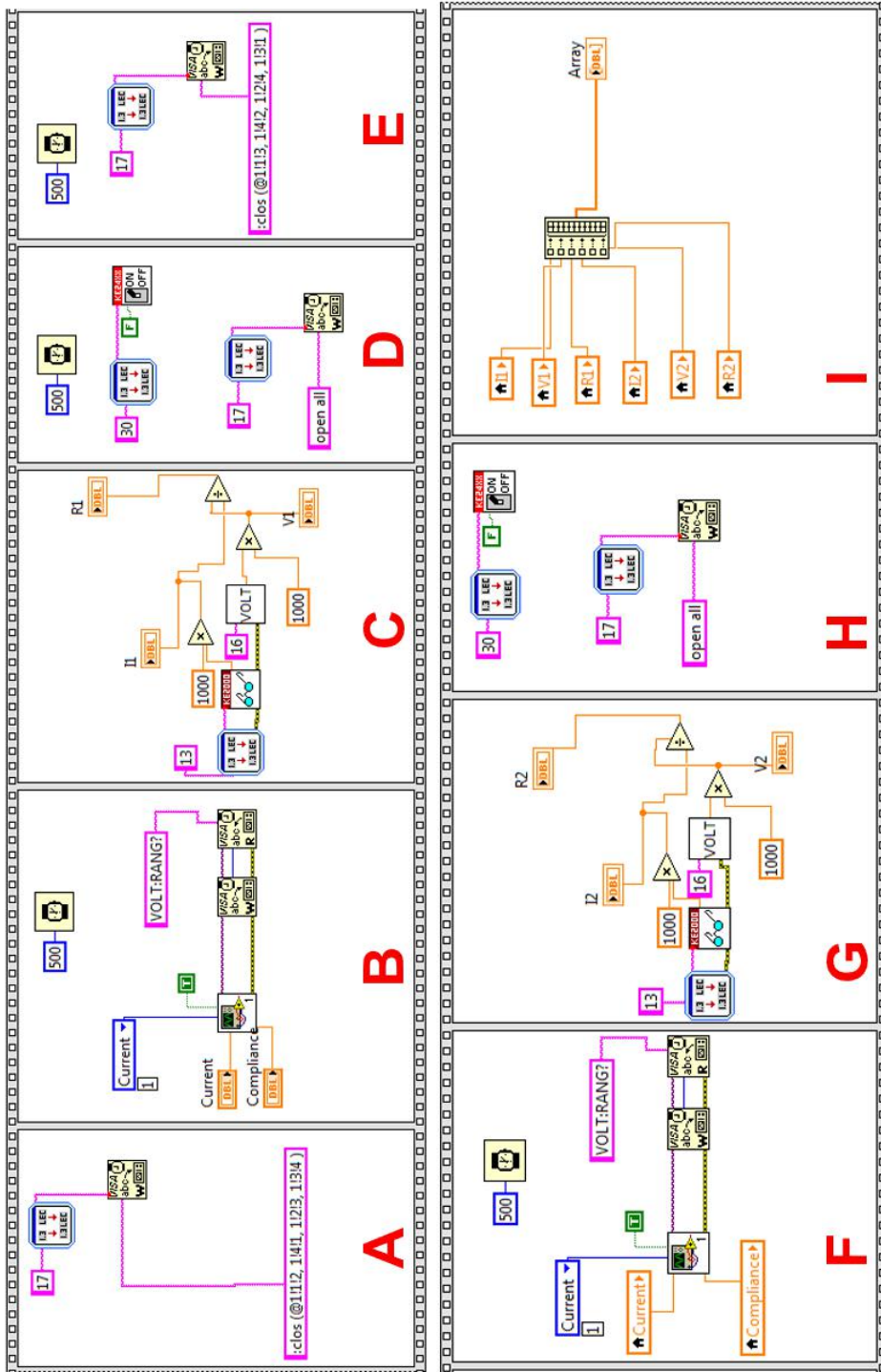


Figure 3.28: Van der Pauw Method - LabVIEW program. The description of each step of this program is detailed below.

- A.** As shown in Figure 3.27, the current is applied through probes 1 and 2 and the voltage is measured between probes 3 and 4. The switch Keithley 7001 closes the corresponding channels to define this functionality in the probes.
- B.** The selected current is applied by the SourceMeter Keithley 2400 between probes 1 and 2.
- C.** The voltage and current are measured between pair of probes 4-3 and 1-2, respectively.
- D.** The SourceMeter Keithley 2400 is turned off and the channels in the switch equipment are opened.
- E.** The switch sets a new configuration for the probes. Probes 2 and 3 for current and 1 and 4 for voltage.
- F.** The selected current is applied by the SourceMeter Keithley 2400 between probes 2 and 3.
- G.** The voltage and current are measured between pair of probes 1-4 and 2-3, respectively.
- H.** The SourceMeter Keithley 2400 is turned off and the channels in the switch equipment are opened.
- I.** The values are saved in an array.

After the values of Voltage, Current and Resistance have been measured, the resistivity is calculated using the Van der Pauw Equation 2.9. A LabVIEW program is designed to solve this equation using an iterative method.

Measure with Modified Van der Pauw method

When Modified Van der Pauw method is selected, an image with the schematic, probes configuration and equation of the method appears in the GUI, as shown in Figure 3.29.

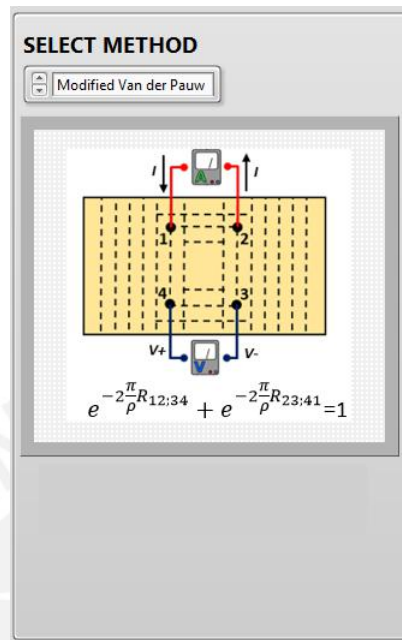


Figure 3.29: Modified Van der Pauw method - schematic, equation and probes configuration.

The procedure to measure the electrical resistivity with this method in the GUI is as follows:

Steps in Calculate resistivity section:

1. Calibrate the camera or use the default value.
2. Place the probes on the sample according to the schematic shown in *Select Method* section.
3. Check continuity with the button VERIFY CONTACTS.
4. Measure the approximate area formed by the four probes pressing the *MEASURE AREA* button.

Steps in Temperature dependence section:

5. Indicate the thickness of the sample, the current and the voltage compliance for the test in *General Parameters* section.
 - **Fixed Temperature mode:**
6. Set the desired temperature and click on the button check in *Measure with Fixed Temperature* section.
7. Click on button *MEASURE RESISTIVITY*.
 - **Variable Temperature mode:**

6. Set initial, step and final temperatures in *Measure with Variable Temperature* section.
7. Choose between *step by step measuring* or *measuring during a set time* in *Measure with Variable Temperature* section.
8. Click on button *START TEMPERATURE TEST*.

The LabVIEW program to calculate the resistivity is similar to the Van der Pauw method. Therefore it is not shown again in detail here. The principal difference is the factor of two in the corresponding equation.

Measure with Linear Van der Pauw method

When Linear Van der Pauw method is selected, an image with the schematic, probes configuration and equation of the method appears in the GUI, as shown in Figure 3.30.

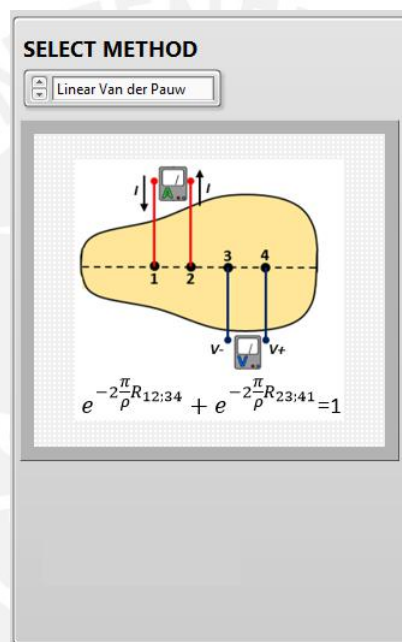


Figure 3.30: Linear Van der Pauw method - schematic, equation and probes configuration.

The procedure to measure the electrical resistivity with this method in the GUI is as follows:

Steps in Calculate resistivity section:

1. Draw a symmetry line pressing the *DRAW SYMMETRY LINE* button.
2. Place the probes in the red line on the sample according to the schematic shown in *Select Method* section.
3. Check continuity with the button *VERIFY CONTACTS*.

Steps in Temperature dependence section:

4. Indicate the thickness of the sample, the current and the voltage compliance for the test in *General Parameters* section.

- **Fixed Temperature mode:**

5. Set the temperature desired and click on the button check in *Measure with Fixed Temperature* section.

6. Click on button *MEASURE RESISTIVITY*.

- **Variable Temperature mode:**

5. Set initial, step and final temperatures in *Measure with Variable Temperature* section.

6. Choose between *step by step measuring* or *measuring during a set time* in *Measure with Variable Temperature* section.

7. Click on button *START TEMPERATURE TEST*.

The LabVIEW program to calculate the resistivity is similar to the Van der Pauw method. Therefore it is not shown again in detail here. The principal difference is the factor of two in the corresponding equation.

Measure with Linear Four Probe method

When Linear Four Probe method is selected, an image with the schematic, probes configuration and equation of the method appears in the GUI, as shown in Figure 3.31.

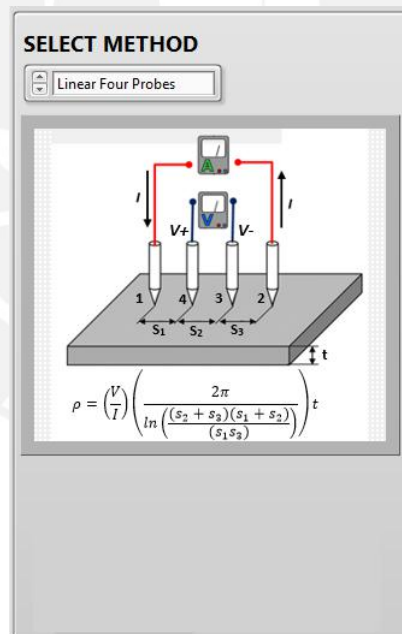


Figure 3.31: Linear Four Probe method - schematic, equation and probes configuration.

The procedure to measure the electrical resistivity with this method in the GUI is as follows:

Steps in Calculate resistivity section:

1. Draw a symmetry line pressing the *DRAW SYMMETRY LINE* button.

2. Place the probes in the red line on the sample according to the schematic shown in *Select Method* section.
3. Check continuity with the button *VERIFY CONTACTS*.
4. Measure distances between the probes pressing *MEASURE DISTANCE* button.
5. Press *CORRECTION FACTOR* button and set the correction factor according to the graph that appears.

Steps in Temperature dependence section:

6. Indicate the thickness of the sample, the current and the voltage compliance for the test in *General Parameters* section.

• **Fixed Temperature mode:**

7. Set the temperature as desired and click on the button check in *Measure with Fixed Temperature* section.
8. Click on button *MEASURE RESISTIVITY*.

• **Variable Temperature mode:**

7. Set initial, step and final temperatures in *Measure with Variable Temperature* section.
8. Choose between *step by step measuring* or *measuring during a set time* in *Measure with Variable Temperature* section.
9. Click on button *START TEMPERATURE TEST*.

The LabVIEW program to calculate the resistivity with this method is shown in Figure 3.32.

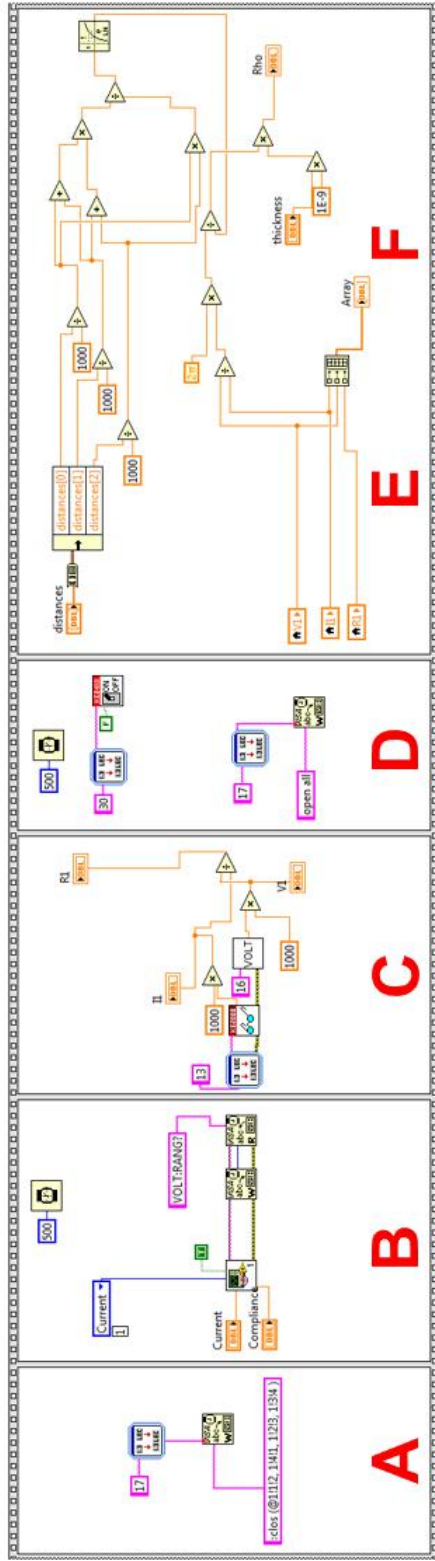


Figure 3.32: Linear Four Probe Method - LabVIEW programming for calculating the resistivity.

- A. The channels are closed in the switch equipment. As shown in Figure 3.31, the current is applied through probes 1 and 2 and the voltage is measured between probes 4 and 3.
- B. The selected current is applied by the SourceMeter Keithley 2400 between probes 1 and 2.
- C. The voltage and current are measured between the pair of probes 1-2 and 3-4, respectively.
- D. The SourceMeter Keithley 2400 is turned off and the channels in the switch equipment are opened.
- E. With the measured values, the resistivity is calculated with the equation shown in Equation 3.2.

$$\rho = \left(\frac{V}{I}\right) \left(\frac{2\pi}{\ln\left(\frac{s_2+s_3}{s_1 s_3}\right)}\right) d \quad (3.2)$$

Chapter 4

Experimental results

This section shows the electrical characterization, as well as, the temperature distribution on the hot side of a Peltier element TEC1-12706. Similarly, the temperature distribution at the surface of the thin film sample is presented below.

The results of resistivity measurements in aluminum and tungsten thin film samples with 100, 300, and 600 nm thickness obtained with the four implemented methods of the measuring system depending on the temperature are also presented in this section.

4.1 Characterization of the Peltier element

The Peltier element is a thermoelectric device which generates a temperature difference between its sides when a current flow is applied to it [32]. For the characterization of the Peltier element, the temperatures of both the hot side and the cold side, along with its corresponding operating voltage were measured. Figure 4.1 shows the temperature behavior of the hot side across a range of voltages during 600 seconds. Values of voltages, ranging from 1 V to 6 V with subdivisions of 1 V were applied in the test, leaving a 1 V safety margin in order to do not reach 411 K, as specified by Peltier TEC1-12706 datasheet. According to the test results, the temperature of the hot side is proportional to the voltage supplied and tends to stabilize in a period of time. The stabilization time will depend on the voltage input, as shown in Figure 4.2. The highest temperature recorded in the test was 373 K when 6 V is applied, and the rate of change for an increment of 1 V was 288 K approximately.

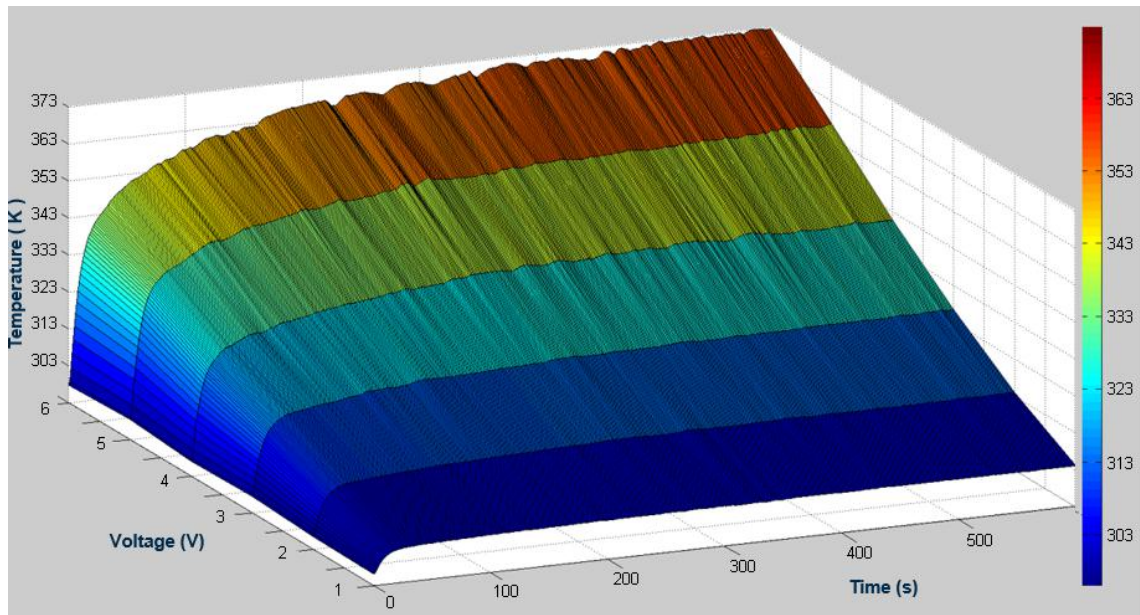


Figure 4.1: Temperature behavior of Peltier element TEC1-12706 hot side across a range of voltages, from 1 V to 6 V, during 600 seconds.

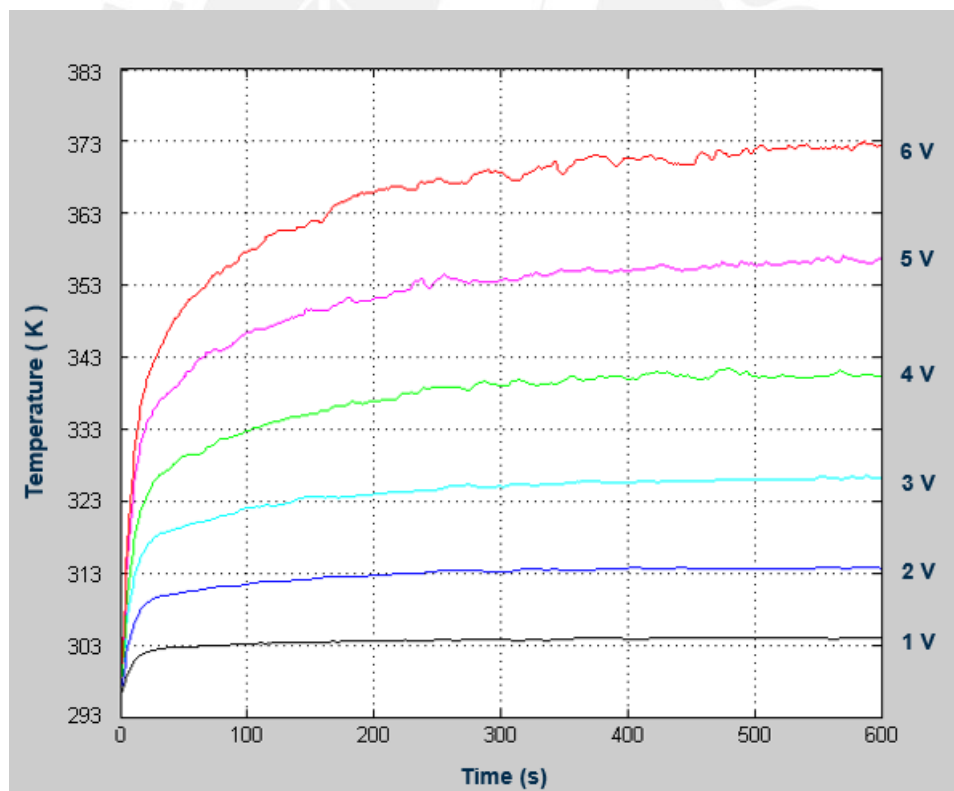


Figure 4.2: Peltier element stabilization time depends on the voltage input and the rate of change for an increment of 1 V is 288 K approximately.

The temperature difference between the hot and the cold sides is shown in Figure 4.3. This temperature difference tends to maintain constant in the time and allows to determine the heat absorption $Q_c(W)$ of the Peltier element. According to Peltier TEC1-12706 datasheet, the maximum heat absorption, Q_{cmax} , is obtained when the temperature difference between the sides is 273 K and $Q_c = 0$ when the temperature difference is 348 K maintaining the hot side at 323 K.

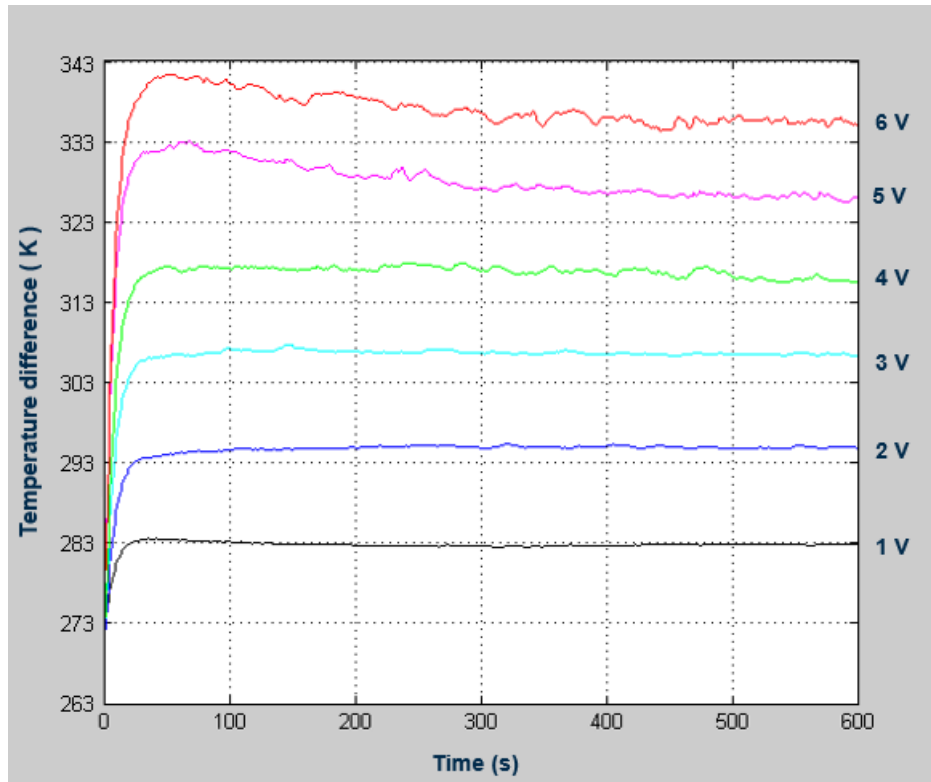


Figure 4.3: The temperature difference between the hot and the cold sides of the Peltier element TEC1-12706.

4.2 Temperature distribution at the surface of the Peltier element

To get an idea of how is the temperature distribution at the hot side of the Peltier element, the temperature was measured at 15 different points at the hot side, as shown in Figure 4.4. Most of the measurements were carried out at the edges of the Peltier element as the highest heat loss by natural convection are located in these areas.

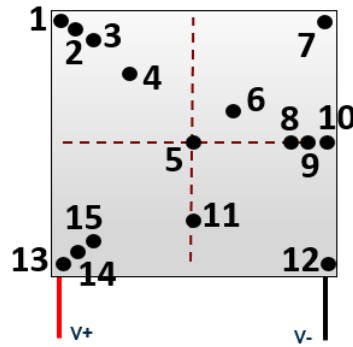


Figure 4.4: Temperature was measured at 15 different points on the hot side to give an insight of temperature distribution.

It is important to ensure that the temperature at the Peltier element hot side gets stable before making the measurements. According to Figure 4.2, when 6 V are applied to Peltier element, the temperature at the hot side gets stable at 373 K. The time to heating up the Peltier until the temperature at the hot side gets stable is 450 s. Figure 4.5 and Figure 4.6 show the temperature distribution at the hot side when 6 V are supplied. It can be seen that the maximum temperature is concentrated at the central part of the hot side and remains uniform in almost all the area with a variation of ± 2 K regarding 373 K. It is also observed that the temperature at the edges of the Peltier is lower by up to 283 K regarding the temperature in the central part. The lower temperatures are located in the area where the Peltier terminals enter. The heat losses at the edges of the Peltier is attributed to the lack of semiconductors in this areas.

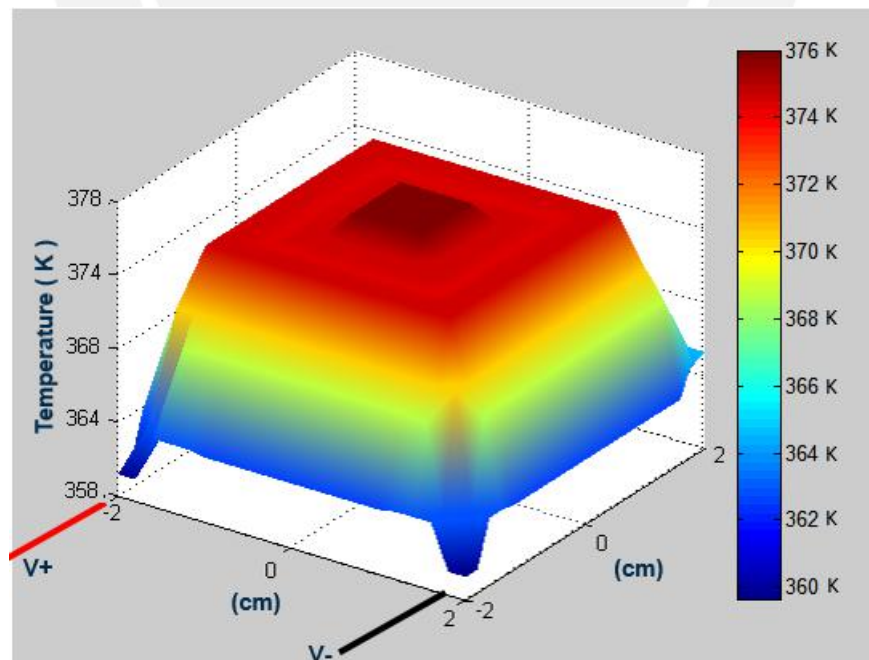


Figure 4.5: Temperature distribution of the hot side when 6 V are supplied to the Peltier element.

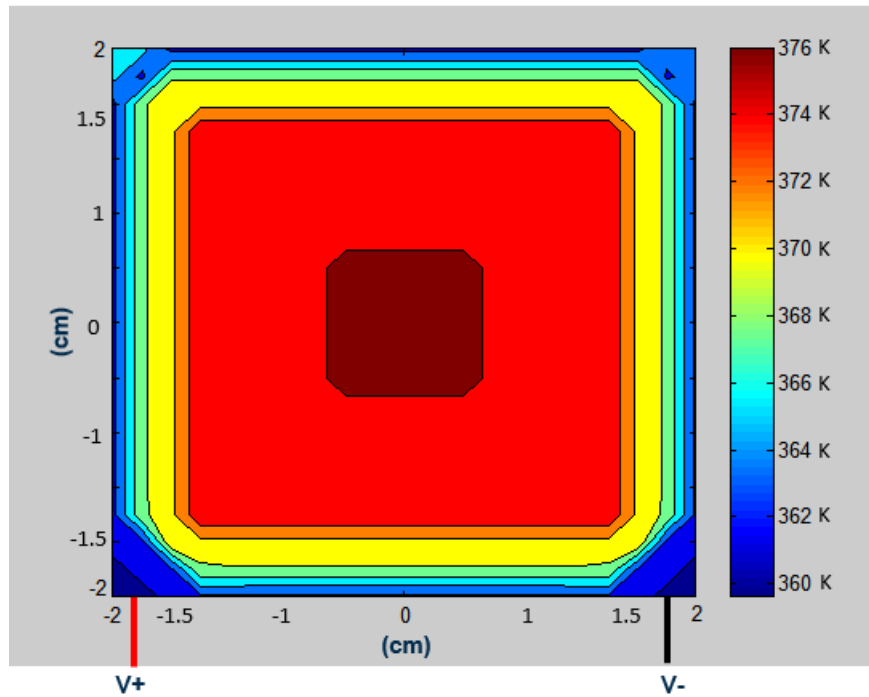


Figure 4.6: The maximum temperature recorded is in the central part. The temperature at the edges is lower than the temperature of the central part due to the lack of semiconductors in the edges.

4.3 Temperature distribution in the sample

The hot side of the Peltier element is used to heat the thin film samples. The dimensions of the Peltier sides are 40 mm x 40 mm, while the samples have a diameter of 50.8 mm. The area in contact between both elements is shown in Figure 4.7A. To obtain temperature distribution of the sample, the temperature was measured at 15 different points at the surface of the sample, as shown in Figure 4.7B.

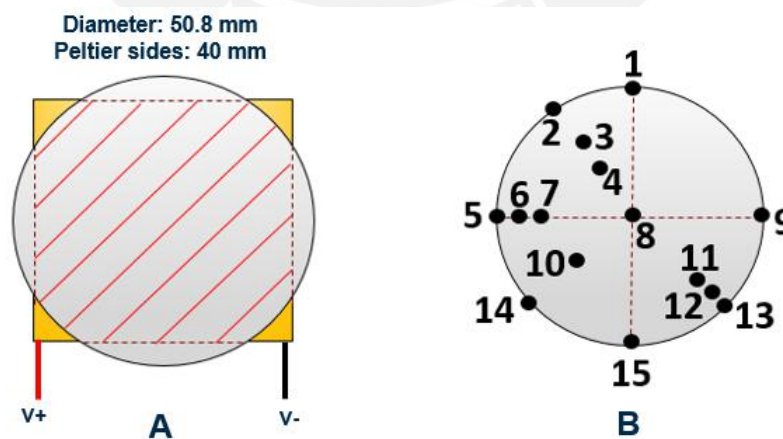


Figure 4.7: **A.** The sample is heated by the hot side of the Peltier element. The red hatched area shows the area of contact between both elements. **B.** The temperature of the sample was measured at 15 different points to give insight of its thermal distribution.

The temperature gets stable in the sample at approximately 373 K when 6 V are applied to the Peltier element. The temperature stabilization time is approximately 454 s. The difference between the temperature stabilization time at the Peltier element hot side and at the surface of the sample is 4 s. This difference indicates that a delay of 4 s has to be taken into account in the system response when a voltage is applied to it. Figure 4.8 shows the temperature distribution of the sample when 6 V were supplied to the Peltier element. The maximum temperature recorded was located in the center of the sample. The temperature remains almost uniform in approximately 85% of the sample area. The edges of the sample record the lowest temperatures with up to 283 K variation regarding the temperature of the central area, as most of the sample's edge area is not in contact with the Peltier element. Moreover, the edge of the Peltier element has the lowest temperatures in its thermal distribution and this influences in the temperature distribution of the sample.

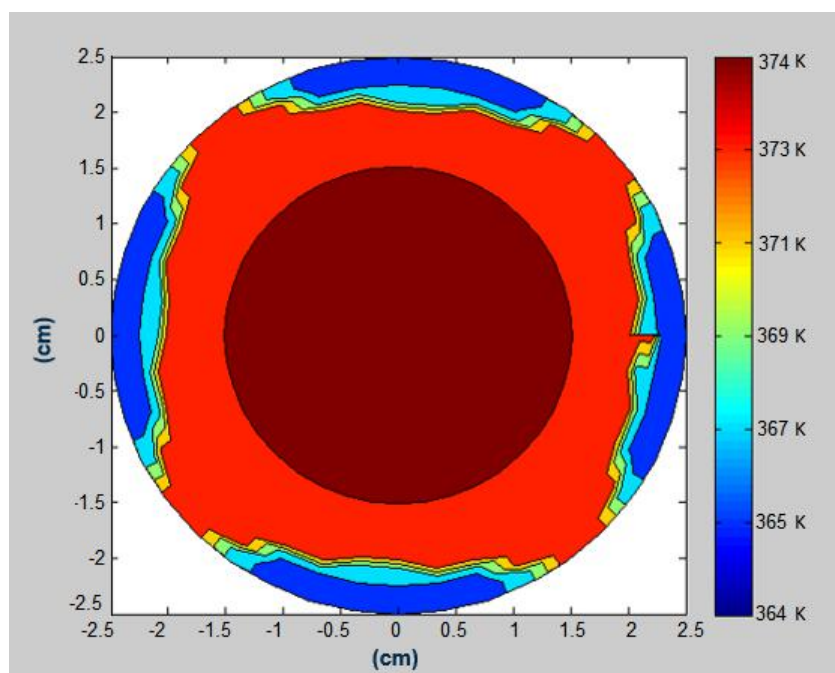


Figure 4.8: Temperature distribution of the sample heated by Peltier element hot side when 6 V is supplied to Peltier element terminals.

Influence of the probes in the temperature of the sample

The temperature was measured in different points close to the contact area between the probes and the sample to determine the influence of the probes in the temperature of the sample. The measurements have been carried out on three different probes configurations, as shown in Figure 4.9.

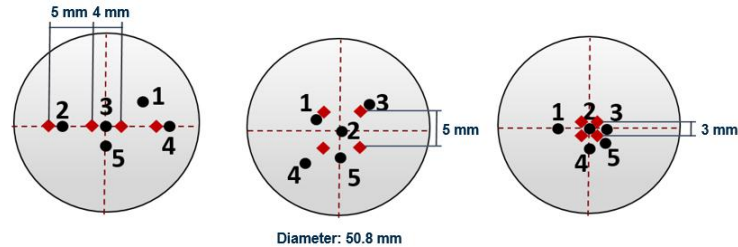


Figure 4.9: Probes configurations to determine the influence of the probes in the temperature of the sample. The red squares represents the four probes and dots with the numbers represents the five measurements carried out with the thermocouple.

Figure 4.10 and Figure 4.11 show the temperature measurements at five different points close to the probes within a temperature range of 303 K to 373 K with increments of 10 K for each configuration. Figure 4.10 shows that the temperature measured close to the probes in the linear configuration is almost equal to the temperature measured at the same point without the probes. Figure 4.11 shows that the temperature measured close to the four probes in a square configuration tends to decrease as the spacing between the probes decreases. For a probes spacing of 5 mm the temperature measured at point 2 decreases by up approximately 1.8 K, while for a probes spacing of 3 mm the temperature in the point 2 decreases by up 3.8 K.

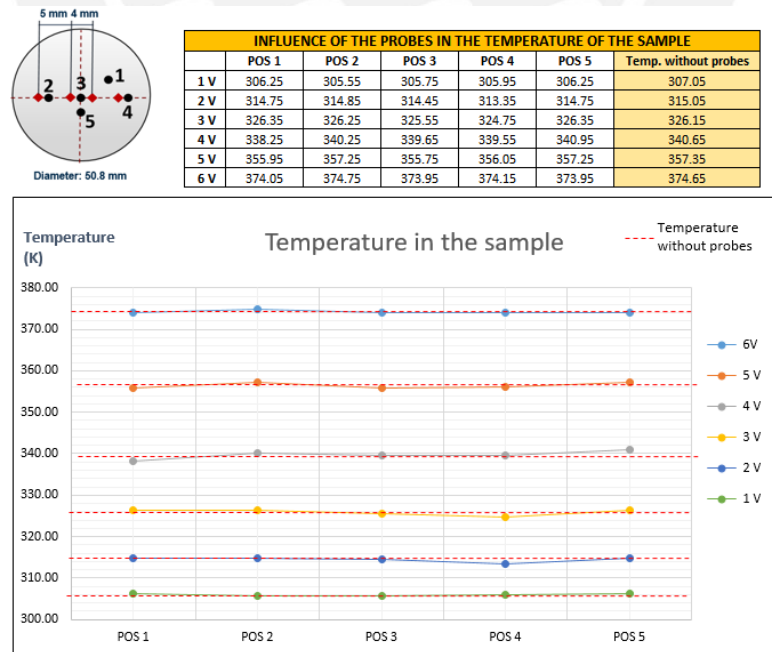
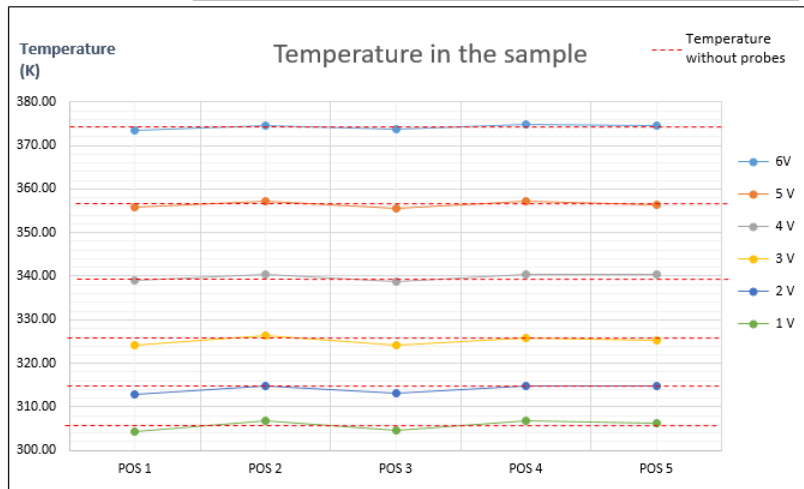
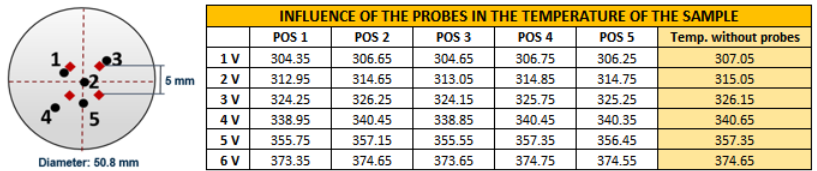
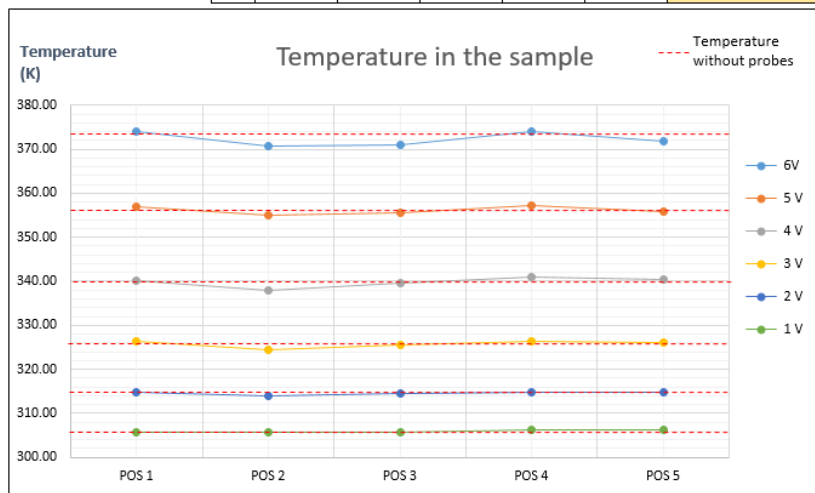
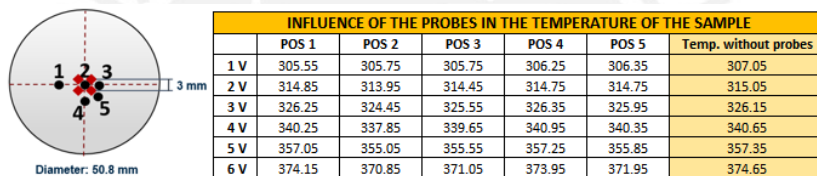


Figure 4.10: Influence of the probes in the temperature distribution of the sample.



(a)



(b)

Figure 4.11: Influence of the probes in the temperature distribution of the sample.

According to the results obtained, the probes do not have a significant influence on the temperature distribution of the sample. However, it is recommended to place the tip of the thermocouple at a distance higher than 3 mm from the probes during resistivity measurements.

4.4 Resistivity measurements results

Resistivity measurements with the four implemented methods have been carried out on aluminum and tungsten thin film samples. In order to show the dependency of the samples resistivity on the temperature, as well as on the film thickness, every measurement was made within a temperature range of 303 K to 373 K with increments of 5 K on thin film samples with 100, 300, and, 600 nm thickness for each material, respectively.

Figure 4.12 shows the resistivity measurements for an aluminum thin film sample with 300 nm thickness using the four implemented methods of the measuring system. Three resistivity measurements have been carried out for every method. The temperature coefficients are shown at the top of every window. Furthermore, it is shown the theoretical temperature coefficient of the aluminum and its corresponding theoretical resistivity values depending on the temperature.

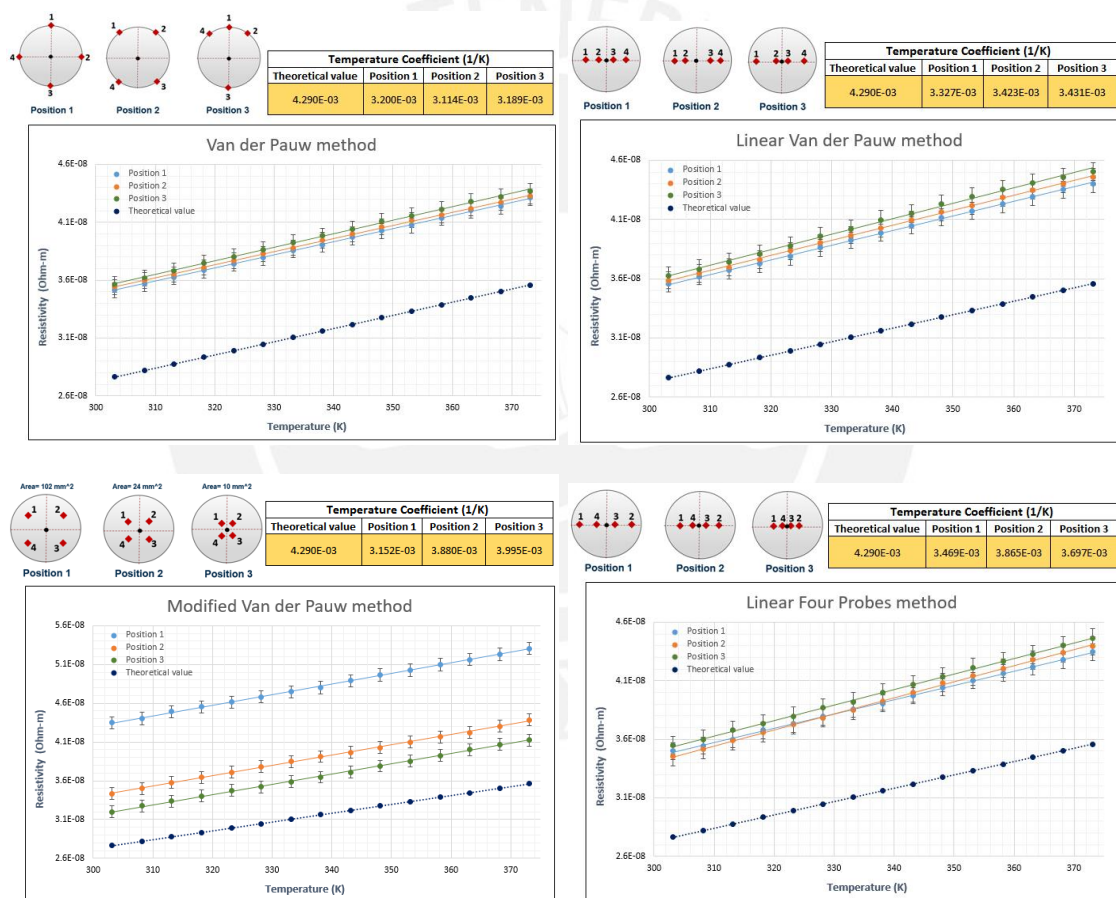


Figure 4.12: Resistivity dependence on the temperature of an aluminum thin film sample with 300 nm thickness. The theoretical temperature coefficient of the aluminum is shown in the tables.

Figure 4.13 shows the comparison of the results obtained with the four methods. According to the results, there is a little difference between the resistivity values in each method. This may be due to probes positioning errors at the edge of the sample in Van der Pauw method, probes misalignment errors in Linear Van der Pauw and Linear Four Probes methods, or geometrical correction factors in Modified Van der Pauw and Linear Four Probes methods.

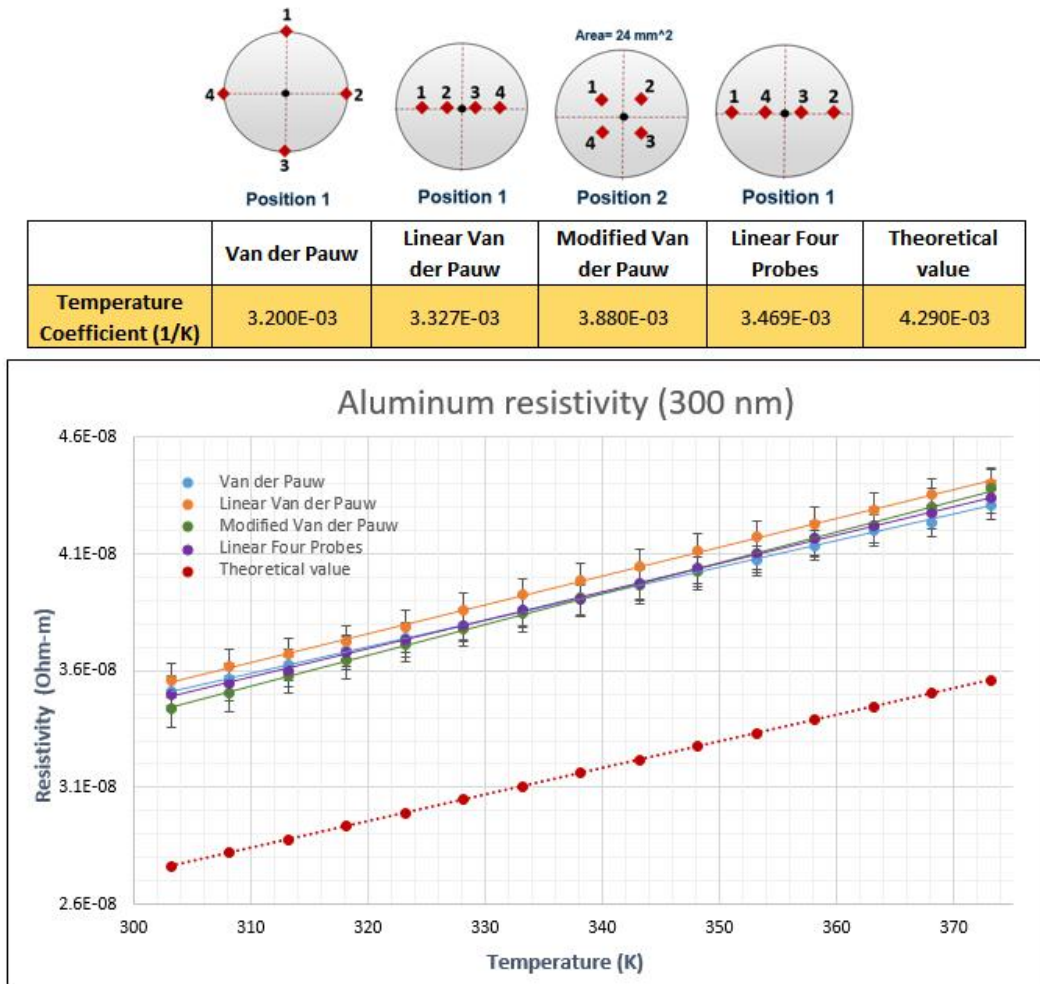


Figure 4.13: Comparison of the results obtained with the four methods at an aluminum thin film sample with 300 nm thickness.

Figure 4.14 shows the resistivity measurements for a tungsten thin film sample with 300 nm thickness using the four implemented methods of the measuring system. The comparison of the results obtained with the four methods is shown in Figure 4.15.



Figure 4.14: Resistivity dependence on the temperature of a tungsten thin film sample with 300 nm thickness. The theoretical temperature coefficient of the tungsten is shown in the tables.

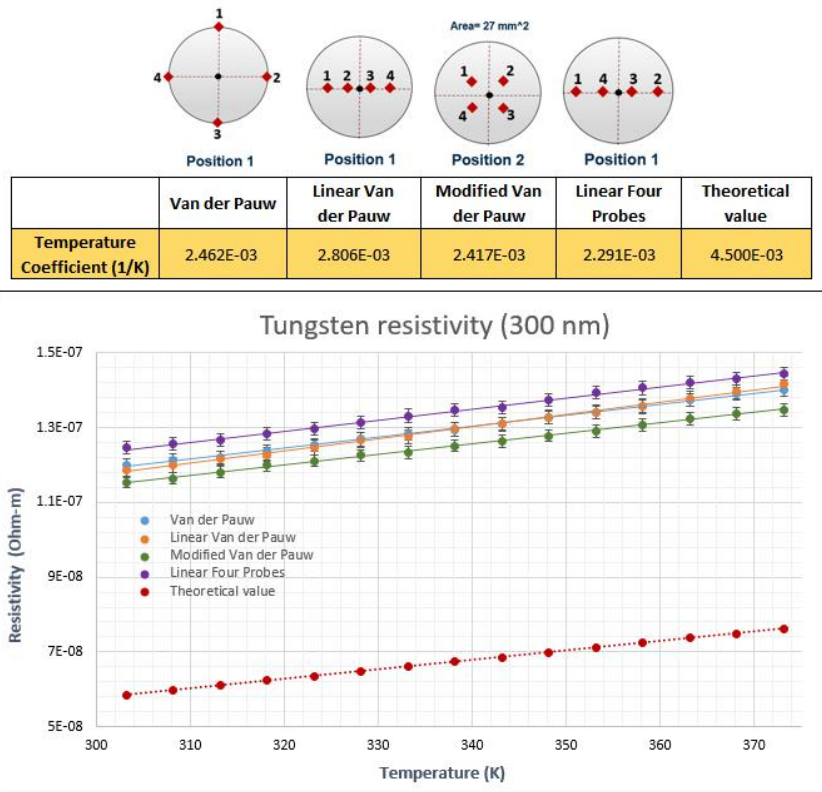


Figure 4.15: Comparison of the results obtained with the four methods at a tungsten thin film sample with 300 nm thickness.

Figure 4.16 shows resistivity measurements for an aluminum thin film sample with 300 nm thickness performed for a heating process as well as for a cooling process using Van der Pauw method. The measurements shows that the resistivity values obtained for both processes are almost the same and that the resistivity of the sample has linear behavior and changes proportionally to the temperature.

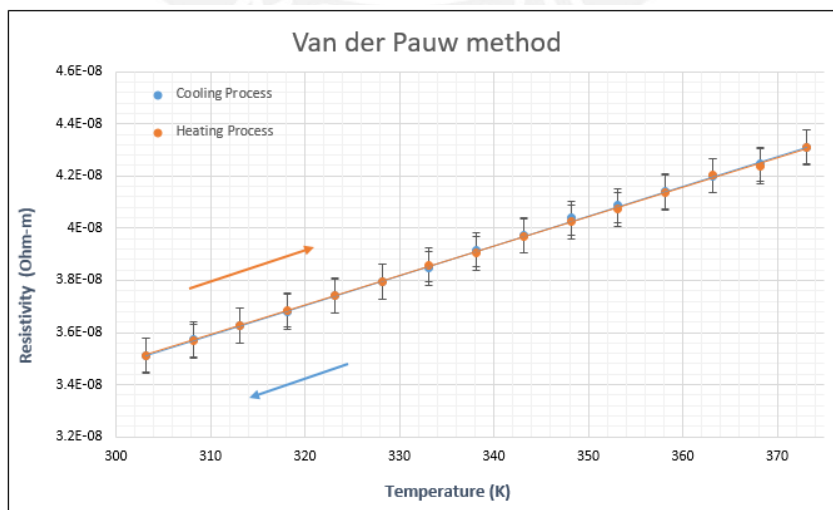
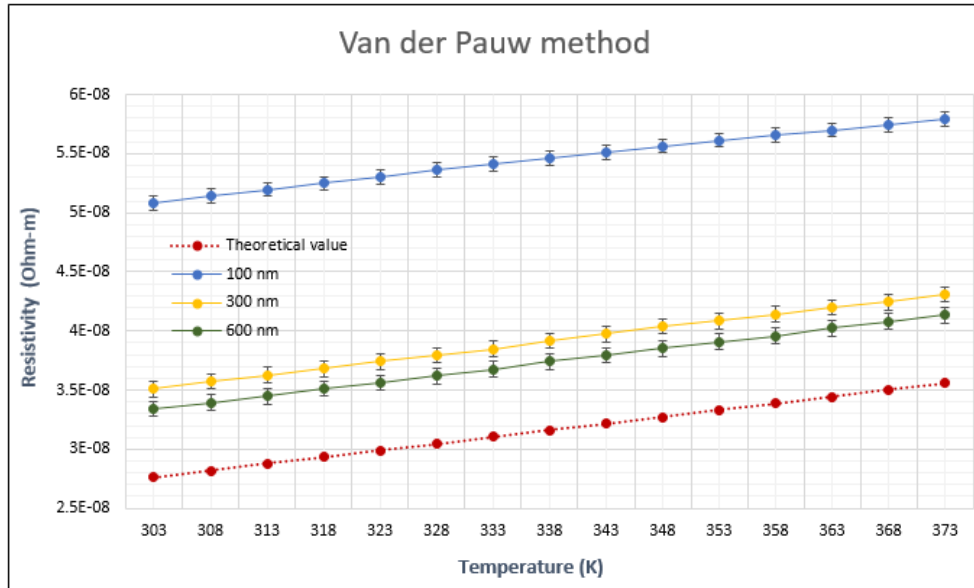
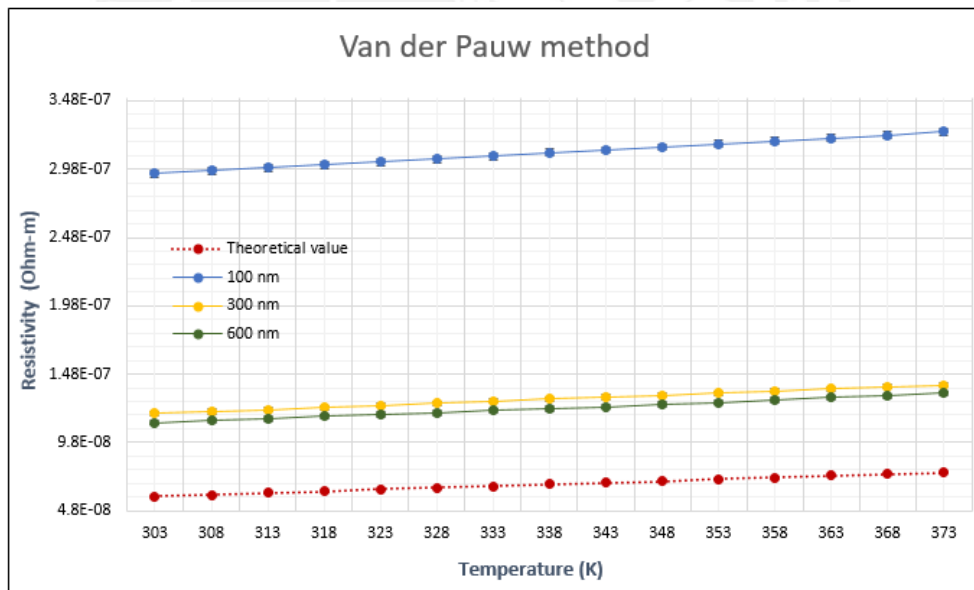


Figure 4.16: Resistivity dependence on the temperature of an aluminum thin film sample with 300 nm thickness.

Figure 4.17 shows the comparison between the resistivity measurements of aluminum and tungsten thin film samples with different thickness. As can be seen, the resistivity values obtained are higher than bulk resistivity, moreover, the resistivity increases as the thickness decreases.



(a) A



(b) B

Figure 4.17: A. Comparison between the resistivity measurements of aluminum thin film samples depending on the temperature with different thickness and its corresponding theoretical values. **B.** Comparison between the resistivity measurements of tungsten thin film samples depending on the temperature with different thickness and its corresponding theoretical values.

Figure 4.18 shows the relation between the resistivity and the thickness of aluminum and tungsten thin film samples. According to the results, the aluminum and tungsten thin film resistivities increases exponentially as the thickness decreases. Furthermore, the resistivity value tends to reach the bulk resistivity value as the thickness increases [46].

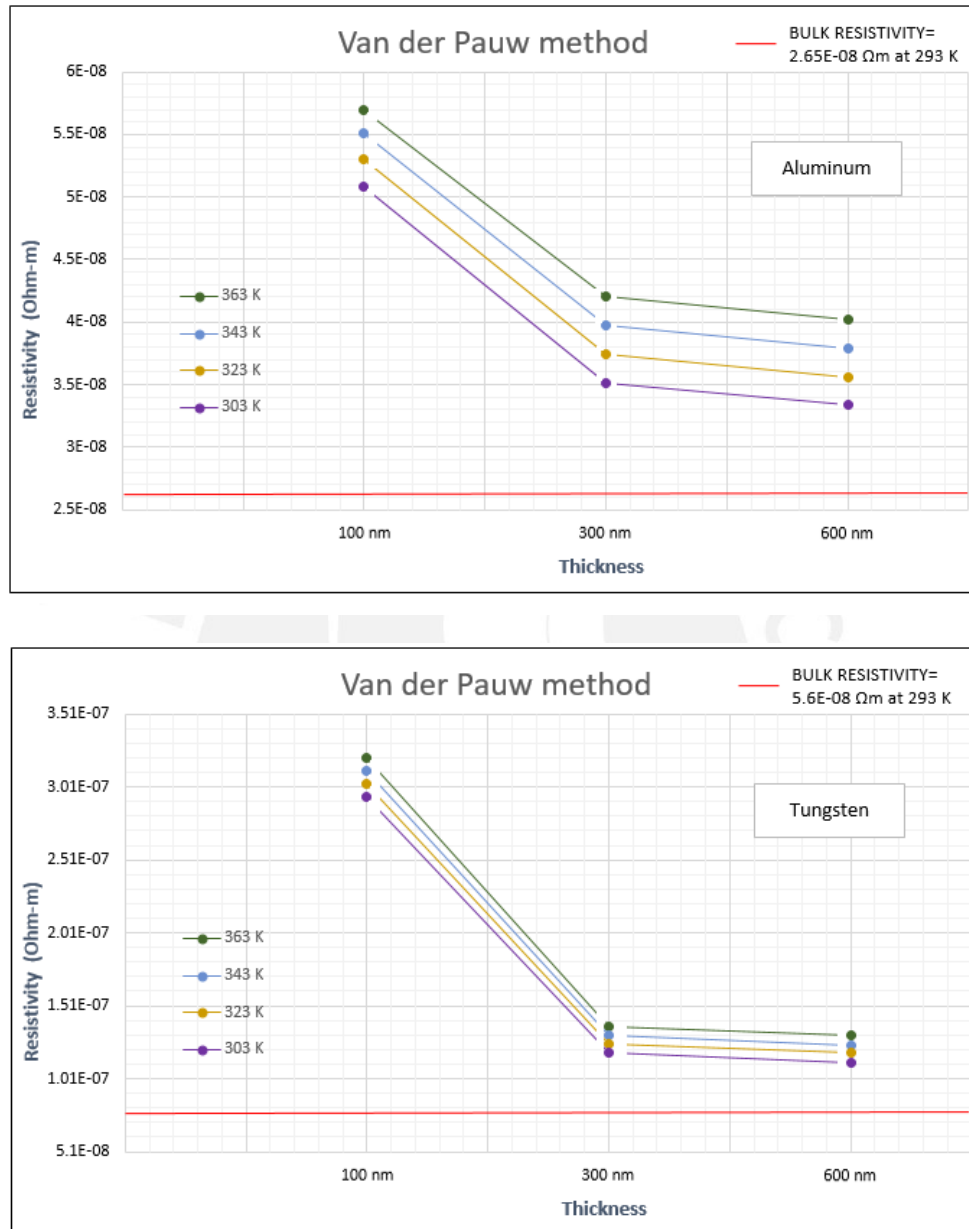


Figure 4.18: **A.**Relation between the resistivity and the thickness of aluminum thin film samples.**B.**Relation between the resistivity and the thickness of tungsten thin film samples.

Figure 4.19 shows the relation between the temperature coefficient and the thickness of aluminum and tungsten thin film samples. The results obtained shows that temperature coefficient increases as the thickness of the sample increases. Moreover, the temperature coefficient of the thin film sample is lower than the bulk value at 293 K and tends to reach this value as the thickness increases [20, 46].

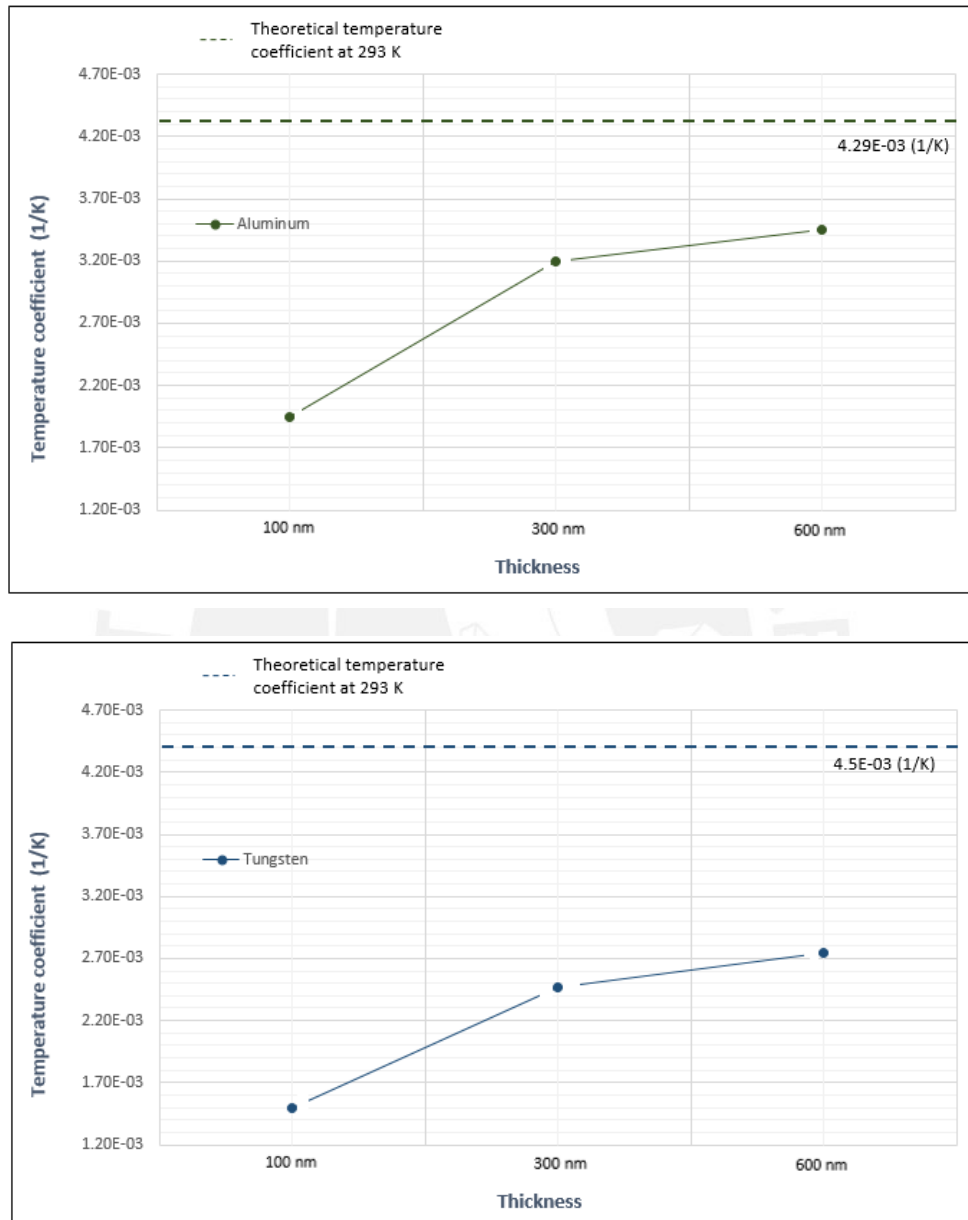


Figure 4.19: **A.**Relation between the temperature coefficient and the thickness of aluminum thin film samples. **B.**Relation between the temperature coefficient and the thickness of tungsten thin film samples.

Chapter 5

Conclusions

A four probes measuring system was implemented to determine the resistivity of thin film samples depending on the temperature, as well as, on the film thickness. Furthermore, a heat source based on a Peltier element was implemented into the measuring system to change the temperature of the sample using different heating rates.

The temperature distribution at the hot side of the Peltier element was characterized. According to the results, the temperature gradient becomes higher as the voltage input increases. The highest temperatures recorded were concentrated in the central part and remains uniform in approximately 80% of the sample's area. The temperature at the edges of the Peltier element decrease by up to 10 K due to the lack of semiconductors in this areas, however, not all this areas are in contact with the sample. The temperature distribution at the surface of the sample was also characterized. The results show that the temperature remains almost uniform in approximately 85% of the area, however, due to the size of the sample and the edges of the Peltier element, the sample's edges present lower temperatures than the central part of the sample with up to 10 K when 6 V are supplied to the Peltier element. These inhomogeneities of the temperature at the sample surface cause errors in the accuracy of resistivity measurements, however, can be neglected due to the resistivity in conductive thin film samples change minimally in a range of 10 K.

Resistivity in aluminum and tungsten thin film samples with 100, 300, and 600 nm thickness depending on the temperature using the four implemented methods were measured. The measurements were performed within a temperature range of 303 K to 373 K with increments of 5 K. The experimental results show that there are little differences between the resistivity results every time the film was measured. This variation in the results are related to probes positioning errors at the surface of the sample and geometrical correction factor.

Resistivity measurements on aluminum and tungsten thin films have been carried out for heating and cooling processes within a temperature range of 303 K to 373 K. The results obtained show that the resistivity values in conductive thin films do not depend on the direction of temperature change.

The resistivity results obtained in both aluminum and tungsten thin film samples are higher than its corresponding bulk resistivity values and increases as the film thickness decreases. This behavior is expected and supported by the theory presented. Moreover, the results show that the temperature coefficients of the measured thin film samples are lower than its theoretical bulk values and increases as the film thickness increases.

Bibliography

- [1] A. A. Ramadan, R. D. Gould, and A. Ashour. On the van der pauw method of resistivity measurements. *Thin Solid Films*, 239(2):272–275, 1994.
- [2] S. H. N. Lim, D. R. McKenzie, and M. M. M. Bilek. Van der pauw method for measuring resistivity of a plane sample with distant boundaries. *Review of Scientific Instruments*, 80(7):075109, 2009.
- [3] Sune Thorsteinsson, Fei Wang, Dirch H. Petersen, Torben Mikael Hansen, Daniel Kjær, Rong Lin, Jang-Yong Kim, Peter F Nielsen, and Ole Hansen. Accurate microfour-point probe sheet resistance measurements on small samples. *Review of Scientific Instruments*, 80(5):053902, 2009.
- [4] Rhett Herman. An introduction to electrical resistivity in geophysics. *American Journal of Physics*, 69(9):943–952, 2001.
- [5] I. Miccoli, F. Edler, H. Pfnür, and C. Tegenkamp. The 100th anniversary of the four-point probe technique: the role of probe geometries in isotropic and anisotropic systems. *Journal of Physics: Condensed Matter*, 27(22):223201, 2015.
- [6] Richard A. Butera and David H. Waldeck. The dependence of resistance on temperature for metals, semiconductors, and superconductors. *J. Chem. Educ.*, 74(9):1090, 1997.
- [7] F. Ashworth and E. D. Taylor. Resistance/temperature coefficients of metals and semi-conductors. *Electrical Engineers-Part I: General, Journal of the Institution of*, 92(59):412–413, 1945.
- [8] George T Meaden. *Electrical resistance of metals*. Springer, 2013.
- [9] Augustus Matthiessen and C. Vogt. Ueber den einfluss der temperatur auf die elektrische leitungsfähigkeit der legirungen. *Annalen der Physik*, 198(5):19–78, 1864.
- [10] Pramond D. Desai, H. M. James, and Cho Yen Ho. Electrical resistivity of aluminum and manganese. *Journal of physical and chemical reference data*, 13(4):1131–1172, 1984.
- [11] Safa O Kasap. *Principles of electronic materials and devices*. McGraw-Hill, 2006.
- [12] R.O. Simmons and R.W. Balluffi. Measurements of the high-temperature electrical resistance of aluminum: Resistivity of lattice vacancies. *Physical Review*, 117(1):62, 1960.
- [13] Lazarus Weiner, Premo Chiotti, and Harley A. Wilhelm. Temperature dependence of electrical resistivity of metals. 1952.

- [14] T. Sorsdal. Determination of standard resistor temperature coefficients. In *Precision Electromagnetic Measurements, 2002. Conference Digest 2002 Conference on*, pages 46–47. IEEE, 2002.
- [15] Christoph Michel, Sergei D. Baranovskii, Peter J. Klar, Peter Thomas, and Bastian Goldlücke. Strong non-arrhenius temperature dependence of the resistivity in the regime of traditional band transport. *Applied physics letters*, 89(11):112–116, 2006.
- [16] JR Sambles. The resistivity of thin metal films—some critical remarks. *Thin Solid Films*, 106(4):321–331, 1983.
- [17] K Fuchs. The conductivity of thin metallic films according to the electron theory of metals. In *Mathematical Proceedings of the Cambridge Philosophical Society*, volume 34, pages 100–108. Cambridge Univ Press, 1938.
- [18] J. Borrajo and J.M. Heras. Validity of approximate equations for the calculation of the electron mean free path in terms of the size effect theory. *Thin Solid Films*, 18(2):267–273, 1973.
- [19] V.V.R. Narasimha Rao, S. Mohan, and P. Jayarama Reddy. Electrical resistivity, tcr and thermoelectric power of annealed thin copper films. *Journal of Physics D: Applied Physics*, 9(1):89, 1976.
- [20] F. Warkusz. The size effect and the temperature coefficient of resistance in thin films. *Journal of Physics D: Applied Physics*, 11(5):689, 1978.
- [21] Yadunath Singh. Electrical resistivity measurements: a review. In *International journal of modern physics: Conference series*, volume 22, pages 745–756. World Scientific, 2013.
- [22] L. Van der Pauw. A method of measuring specific resistivity and hall effect of discs of arbitrary shape. *Philips Res. Rep.*, 13:1–9, 1958.
- [23] Egbert Hesse. A four-point probe method with increased accuracy for the local determination of the thickness of thin, electrically conducting layers. *IEEE Transactions on Instrumentation and Measurement*, 1001(3):166–175, 1982.
- [24] Leopoldo B. Valdes. Resistivity measurements on germanium for transistors. *Proceedings of the IRE*, 42(2):420–427, 1954.
- [25] Akira Shimamoto, Keitaro Yamashita, Hirofumi Inoue, Sung-mo Yang, Masahiro Iwata, and Natsuko Ike. A nondestructive evaluation method: measuring the fixed strength of spot-welded joint points by surface electrical resistivity. *Journal of pressure vessel technology*, 135(2):021501, 2013.
- [26] David S Perloff. Four-point sheet resistance correction factors for thin rectangular samples. *Solid-State Electronics*, 20(8):681–687, 1977.
- [27] John Albers and H. L. Berkowitz. An alternative approach to the calculation of four-probe resistances on nonuniform structures. *Journal of the Electrochemical Society*, 132(10):2453–2456, 1985.
- [28] F.M. Smits. Measurement of sheet resistivities with the four-point probe. *Bell System Technical Journal*, 37(3):711–718, 1958.
- [29] Donald M Mattox. *Handbook of physical vapor deposition (PVD) processing*. William Andrew, 2010.

- [30] Micro Magnetics. Magnetron sputtering technology. <http://www.directvacuum.com/pdf>, 1999. Accessed: 01-02-2017.
- [31] Mohamed Guiatni, Abdelhamid Drif, and Abderrahmane Kheddar. Thermoelectric modules: Recursive non-linear arma modeling, identification and robust control. In *Industrial Electronics Society, 2007. IECON 2007. 33rd Annual Conference of the IEEE*, pages 568–573. IEEE, 2007.
- [32] Philippe M Beaudoin, Yves Audet, and Abdelhalim Bendali. Characterizing a thermoelectric module as part of a semiconductor course laboratory. *IEEE Transactions on Education*, 51(2):282–287, 2008.
- [33] Nanophotonics Group Ludwig Maximilian University of Munich. The fundamentals of thermoelectrics. <http://www.nano.physik.uni-muenchen.de>. Accessed: 01-02-2017.
- [34] Simon Lineykin and Shmuel Ben-Yaakov. Modeling and analysis of thermoelectric modules. *IEEE Transactions on Industry Applications*, 43(2):505–512, 2007.
- [35] David Michael Rowe. *Thermoelectrics handbook: macro to nano*. CRC press, 2005.
- [36] William Bolton. *Instrumentation and control systems*. Newnes, 2015.
- [37] Graham Clifford Goodwin, Stefan F. Graebe, and Mario E. Salgado. *Control system design*, volume 240. Prentice Hall New Jersey, 2001.
- [38] Keithley. 2400 series source meter user’s manual. *Seventh Printing, Cleveland, Ohio, USA*, 2002.
- [39] Keithley. Model 2000 multimeter user’s manual. *Eighth Printing, Cleveland, Ohio, USA*, 2003.
- [40] Keithley. Model 7001 switch system quick reference guide. *Cleveland, Ohio, USA*, 1992.
- [41] PeakTech Pruef und Messtechnik GmbH. Peaktech 1575 operation manual.
- [42] Keithley. Model 2001 multimeter operator’s manual. *Seventh Printing, Cleveland, Ohio, USA*, 1999.
- [43] Keithley. Model 2002 multimeter operator’s manual. *Seventh Printing, Cleveland, Ohio, USA*, 1999.
- [44] Gianluca A. Mannella, Vincenzo La Carrubba, and Valerio Brucato. Peltier cells as temperature control elements: Experimental characterization and modeling. *Applied thermal engineering*, 63(1):234–245, 2014.
- [45] B.J. Huang and C.L. Duang. System dynamic model and temperature control of a thermoelectric cooler. *International Journal of Refrigeration*, 23(3):197–207, 2000.
- [46] Yoshikatsu Namba. Resistivity and temperature coefficient of thin metal films with rough surface. *Japanese Journal of Applied Physics*, 9(11):1326, 1970.